Compatibility Evaluation of Glass/Epoxy Insulation for Use in ITER's Central Solenoid Superconducting Electromagnets

A Thesis Presented for the
Master of Science
Degree
The University of Tennessee, Knoxville

Carolyn Grace Kidwell
May 2012

ACKNOWLEDGEMENTS

I would first like to express my complete gratitude to my advisor Dr. Mahdu Madhukar for his guidance and support throughout this project. Without his encouragement and instruction, I would not have been able to complete this study. I would also like to thank the rest of my committee members, Dr. Kevin Kit and Dr. Hahn Choo, for their time and the advice given to help improve the quality of this study.

It is also necessary to express the deep appreciation I have for the constant help given to me by all of the guys at the Magnet Development Laboratory. Without their help machining the equipment used as well as samples studied, none of the research completed would have been possible. They were always willing to help with any problem solving throughout this process and played a key role in the success of this project.

I would also like to express my gratitude to ITER for the financial support they provided to make this project possible. There were also many members of the ITER staff that provided input to help complete this study.

A big thanks is also needed for my fellow graduate student working for Dr. Madhukar, Anupont Thaicharoenporn, for providing the data for the neat resin samples and always bringing a smile in the midst of all this research. I would also like to thank my other fellow graduate students, Max Trent and Josh Burgess, for their support and encouragement throughout this process. I am also very

appreciative of Greg Jones who played a big role in helping me obtain the SEM photographs.

I cannot express how grateful I am for my friends and family I have been blessed with. The nonstop encouragement and support given to me was, at times, the only thing that kept me going. I specifically want to thank my mother for all her input and guidance, as well as, always providing me a place to get away to so that I could focus.

Most importantly, I owe all of my accomplishment in this study to God. Without the abilities he blessed me with, this project would have been impossible for me. I could not be more thankful for the blessings he has placed in my life and for his constant provision through it all.

ABSTRACT

A variety of glass fiber types are being considered for use as insulation material in the central solenoid superconducting electromagnets for the International Thermonuclear Experimental Reactor (ITER). Before these materials can be used, a compatibility of these glass products with an epoxy matrix has to be characterized. In this study, three candidate glass types (1581, 7781, and 38050) were considered and their compatibility with a DGEBF epoxy matrix was determined via three-point flexure tests at room temperature (295K) and liquid nitrogen temperature (77K) and constant load flexure creep tests at room temperature. The material variables among these glass products were – type of weave pattern (8-harness satin versus plain), fiber surface treatment (epoxy compatible surface treatment versus no treatment), and cloth density. Based on the stiffness and strength data at both 77K and 295K, the 7781/epoxy composites showed the highest values followed closely by 1581/epoxy. However, 38050/epoxy performed quite poorly. Evidence in an increase of interfacial strength as the temperature was lowered to 77K was seen through examination of the failure pattern. The correlations of the glass cloth density and fiber volume fraction with stiffness and strength at both temperatures were almost linear. It was also found that the failure modes of samples having fibers with epoxy compatible surface treatment differed from those having no surface treatment. Constant load flexural creep tests showed that the 7781/epoxy composites performed the best with the least amount of strain at higher loads than the other types of composites. The 1581/epoxy composite followed with the 38050 again performing quite poorly.

TABLE OF CONTENTS

LIST OF TABLES

Table Page

LIST OF FIGURES

List of Figures: Appendix I

List of Figures: Appendix II

CHAPTER I
INTRODUCTION AND GENERAL INFORMATION

The International Thermonuclear Experimental Reactor (ITER) is an international research and engineering project which is currently building the world's largest and most advanced experimental tokamak nuclear fusion reactor in Europe, at Cadarache in the south of France. One of the main components of the ITER magnet system is the Central Solenoid (CS), which consists of six independent coil pack units that use a Niobium-Tin (Nb_3Sn) Cable-in-Conduit superconducting conductor held together by a vertical precompression structure [1]. Each of the six units will be manufactured independently and consist of stacked pancake like layers that are bonded together with an epoxy-glass composite structure. This structure is fabricated using the vacuum-pressure impregnation (VPI) technique to transfer the resin into the prewound glass within the structure. Each unit will weigh about 110 metric tons. The dimensions of each module will be about 2.1 m high with an outer diameter of 4.2 m and an inner diameter of 2.7 m. The conductors in each unit and units themselves have to be insulated so as to provide these units a high voltage (up to 29 kV) operating capability [2]. In addition to providing the electrical insulation, the conductor jacket material has to resist the large electromagnetic forces arising during operation and be able to demonstrate good fatigue behavior. Several glass-epoxy insulation materials are being considered for this purpose.

There are two types of insulation in CS coil – turn insulation and ground insulation. The turn insulation consists of wrapped cowound Kapton and glass tape around all stainless steel conduits that encompasses the superconductor. The ground insulation includes glass cloth, Kapton sheet, and glass/epoxy high-pressure laminate.

Both types are bonded by epoxy resin that is transferred into the glass tape and cloth following assembly through the VPI resin-transfer process. The resin selected for use in the CS coil units is composed of DGEBF epoxy with an anhydride hardener and a very small amount of accelerator.

Various types of fiber weaves are being considered for use in CS insulation. One of the most important requirements for the glass fibers is that they should have good adhesion (compatibility) with the epoxy being used. In this study, three types of E glass tape/cloth were chosen to determine and compare their compatibility with DEGBF epoxy. These glass products differed in type of weave pattern, aerial density of glass cloth/tape, and fiber surface treatment. The compatibility between the glass fibers and epoxy was evaluated through testing the strength and stiffness of each composite laminate and examining the fracture surface. This study will also begin a look at the creep behavior of the three different laminates as a way to further compare the compatibility between the glass fibers and the epoxy. The Nb_3Sn material used in the CS coils is superconducting at liquid helium temperature (4K). Therefore, it is important to characterize the insulation material at these

temperatures. However, due to handling difficulties of liquid helium, it was decided to characterize the material at liquid nitrogen (77K) instead.

CHAPTER II
LITERATURE REVIEW

Considerations for Glass Fiber

Surface Treatment

The interface between the fiber and the matrix is a highly studied area due to the properties of the composite being largely controlled by this region. This region has different properties than either the fiber or the matrix and can greatly influence the overall strength of the composite [3]. In order to get the most use out of a reinforcing material, a good interface bonding that will allow load transfer from the matrix to the reinforcement is necessary [4]. The general consensus is that higher bond strength improves mechanical properties, provided the improved bond strength does not produce a brittle interphase [3-10]. A main factor when looking at the interface region is the surface coating on the fibers applied by the manufacturer [5]. A key component to the surface coating is the silane coupling agents because it promotes the adhesion between the fiber and the matrix. Chemical bonding and a network created between reactive organic functional groups in the silane on the surfaces of the fiber and matrix are believed to cause strong interfacial interactions between the fiber and the matrix [3]. While adding the silane surface treatment increases the overall strength, it is important to make note that an increase in the strength of the composite typically produces a decrease in fracture toughness [3-5].

Type of Weave

While there have been several studies on the effect of fiber surface treatment on the composite properties [3-10], the studies on the effect of weave pattern on composite properties have been few [11,12]. The most commonly used weave patterns in composite materials applications are plain and satin weaves. In plain weave, each warp fiber tow passes alternately under and over each weft fiber making the fabric symmetrical as seen in Figure 1a. The plain weave provides good stability, porosity and the least yarn slippage for a given yarn count. However, the higher level of fiber crimp imparts relatively low mechanical properties compared with the other weave styles. A satin weave, in particular 8-harness satin weave, is the most widely used in the composites industry due to its ability to produce minimal distortions when forming over curved surfaces. In 8-harness satin weaves, each filling yarn floats over seven warp yarns and under one as seen in Figure 1b. The low crimp in satin weaves gives them better mechanical properties compared to those in plain weave. With the 38050 plain weave pattern, both planar directions have the same pattern (Figure 2a), but with 8-harness satin weaves (7781 and 1581) the breaking strengths are different in warp and fill directions (see Table 1). The 7781 cloth and 1581 tape are similar in the fact that they have the same weave pattern and surface finish, but what distinguishes them is the yarn used to create the weave. While the thread count is the same and the weight difference is almost negligible (7781 = 295.32 g/m^2, 1581 = 290.91 g/m^2), the 7781 fabric is woven with ECG 7510 yarn and the 1581 fabric is woven with ECG 1512 yarn. The ECG 1512 yarn is a two-strand yarn that is twisted together to form one larger strand while the ECG 7510 yarn is a single strand (Figure 2). The linear density of the

ECG 7510 is twice that of a single strand of the ECG 1512, so when two of the later are twisted together, the dimensions and weights of fabrics woven in the same pattern with these two yarns will be similar [13].

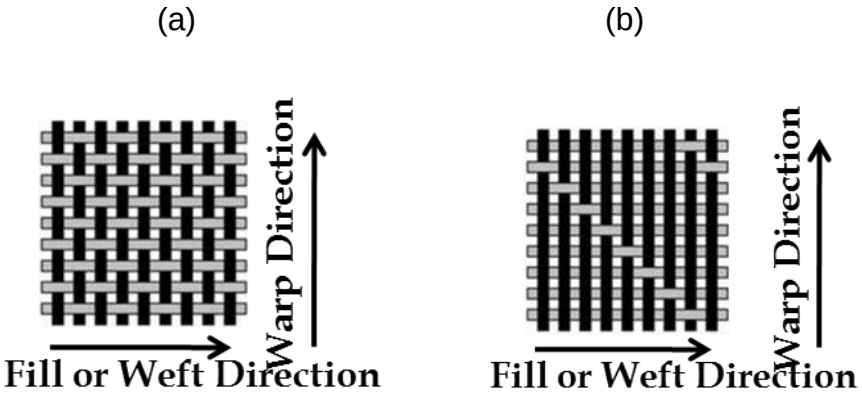

Figure 1. Schematics of a) a plain weave and b) an 8-harness satin weave.

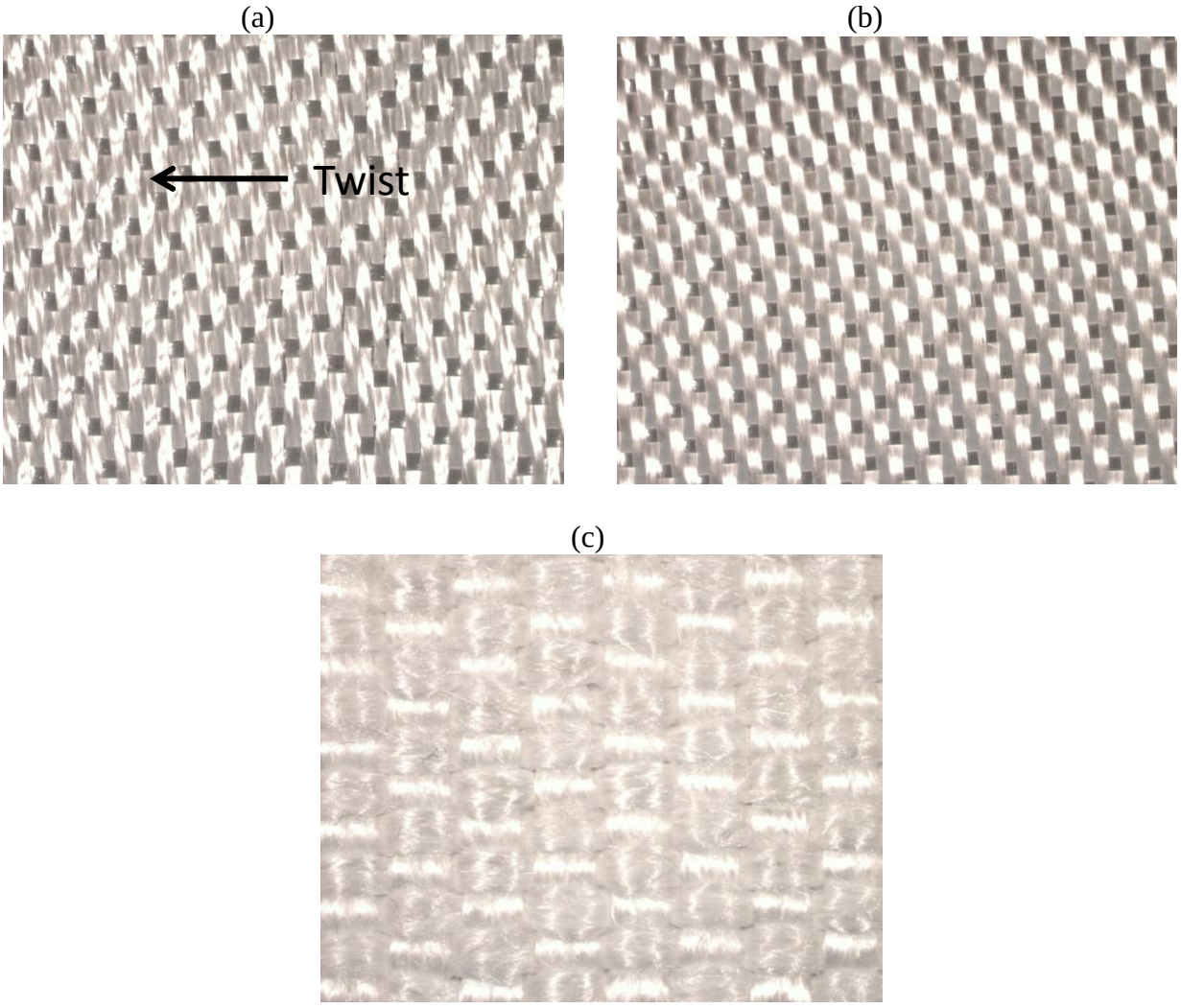

Figure 2. Photographs of the three glass fibers used in this study (a) 1581 (b) 7781 (c) 38050.

3-Point Flexure Test

The 3-point bend test was chosen for the compatibility study because generally in this test the data scatter is much lower compared to other tests such as uniaxial tension, compression, or interlaminar shear [6]. The reason being that in the 3-point bend test the localized region around the middle of the sample is under maximum stress, and, hence, the failure always starts there compared to other tests in which the state of stress is uniform throughout the sample and the failure starts at the weakest point. Additionally, specimen gripping for low temperature tests is considerably easier and no tests are discarded based on laminate failures at the grips.

The ratio of span length (distance between outer two contact points)-to-thickness (sample thickness in the loading direction) can be adjusted. Long span-to-thickness ratios result in the dominance of bending stresses over the interlaminar shear stresses at the point of flexure. Small span-to-thickness ratios result in the dominance of interlaminar shear. With careful adjustment of the ratio, a desired failure mode can be produced in the composite samples [14].

Creep

Creep of a material occurs when a stress less than the strength of the material is applied causing the material to deform over time. The typical behavior of a material experiencing creep can be seen in Figure 3. There are three stages of creep: primary, secondary, and tertiary. In the initial stage of creep, the strain rate is initially high, but

slows as time passes. The secondary stage of creep, also known as steady-state, is characterized by a liner increase in strain with time meaning there is a constant strain rate. The final stage of creep, tertiary, has a rapid increase in strain followed by creep rupture [15].

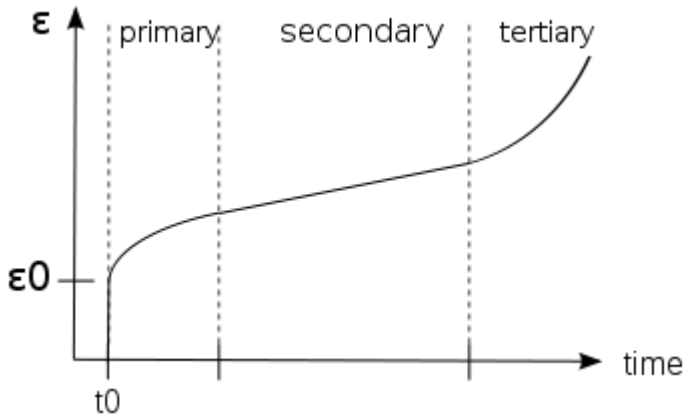

Figure 3. Strain as a function of time due to constant stress over an extended period for a viscoelastic material.

In a composite material with a polymer matrix and a glass fiber, the creep occurring in the material will mainly occur in the matrix. For polymeric materials, the creep mechanism caused by a load placed on the material can be described by the movement of molecules [17,18]. When a constant load is placed on a polymeric material for a period of time, the material will deform by the distortion of the bonds and/or by rearranging the atoms. These deformations will then lead to changes in the molecular chains of the polymer as a load is experienced on the material. In unordered regions of the polymer, uncoiling, straightening, and breaking can be seen, while slippage between chains will be seen in an ordered region of the polymer. It has been shown that with an

increasing load, the creep rate in the secondary stage increases, a decrease in the rupture lifetime is seen, and the instantaneous strain experienced by the material at the initial application of the load increase [16-18].

It is important to look at the time dependent mechanical properties of materials due to the difference that can be seen from short term properties [19]. Because of its experimental convenience and applicability in common loading configurations, constant load creep was chosen for this study.

CHAPTER III
MATERIALS AND METHODS

Material

The three glass types evaluated in this study were 38050, 7781, and 1581. All glass products were obtained from Carolina Narrow Fabric. The 38050 is an untreated E-glass plain weave that doesn't have an epoxy compatible (usually silane) finish. It was obtained in 51 mm wide, 1.0 mm thick tapes. Both 7781 and 1581 are 8-harness satin weave E-glass. The 7781 and 1581 are quite similar except 7781 has a flatter weave (due to difference in the yarn used) than 1581 which gives it a higher glass to resin ratio and a higher breaking strength. While the glass fibers in 38050 are untreated, the fibers in 7781 and 1581 have an epoxy compatible silane finish. Table 1 below summarizes data related to these glass products.

Table 1. Types of Glass Cloths/Tapes used.

Type of Glass	Ply Thickness	Form	Areal Density (gm/cm^2)	Weave Type	Strength N/m	Surface Treatment
38050	1.00 mm	51 mm wide tape	0.089	Plain	Not available	Untreated
7781	0.23 mm	cloth	0.0304	8-harness satin	Warp: 42.4 Fill: 40.5	Epoxy compatible treatment
1581	0.23 mm	51 mm wide tape	0.0306	8-harness satin	Warp: 34.7 Fill: 30.6	Epoxy compatible treatment

The type of resin used was DGEBF epoxy with an anhydride hardener that was obtained from Huntsman Corporation [13]. The mixing ratios for the resin are given in Table 2.

Table 2. Epoxy components and their mixing ratios.

Component	Parts by weight	Commercial designation
DGEBF epoxy	100	Araldite GY 282
MTHPA hardener	82	Aradur 918
accelerator	0.25	DY 073-1

Fabrication of Composite Samples

The composite samples were made using the vacuum pressure impregnation (VPI) technique which involved several preparatory steps.

Sample Geometry

A mold was designed to accommodate the three types of glass material in a rectangular cavity. The arrangement of the glass cloth/tapes is shown in Figure 4. The number of plies was chosen in such a way so that the final thicknesses of the impregnated parts were around 2 mm.

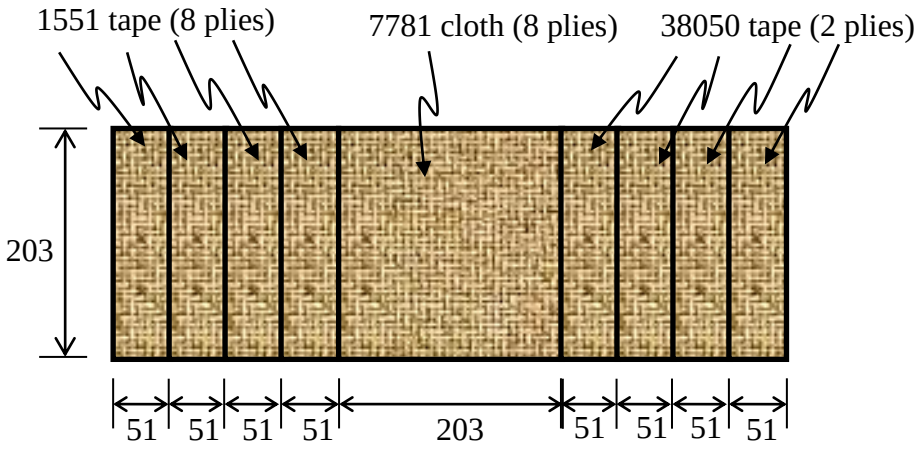

Figure 4. The arrangement of the three types of glass placements in the mold cavity. Dimensions are in mm.

Mold Design

The sample mold essentially consisted of two sealed rectangular aluminum plates. One of the plates (plate A, Figure 5) had a 2.2 mm deep rectangular cavity inside it to place the glass samples. There was a through-the-thickness ¼ in pipe tap thread hole machined at one of the corners of the cavity for resin outlet. The assembled sample mold would be placed in the sample vacuum tank in a position such that the resin enters the mold at its lowest point. There was also a groove machined around the outside edge of the rectangular cavity for the placement of an O-ring to prevent the resin from leaking out of the cavity (Figure 6). Threaded holes were machined around the edge of the plate to bolt the two plates together. On the outside surface of and in the middle of plate A was a small recess to attach a thermocouple. This thermocouple will monitor the sample temperature.

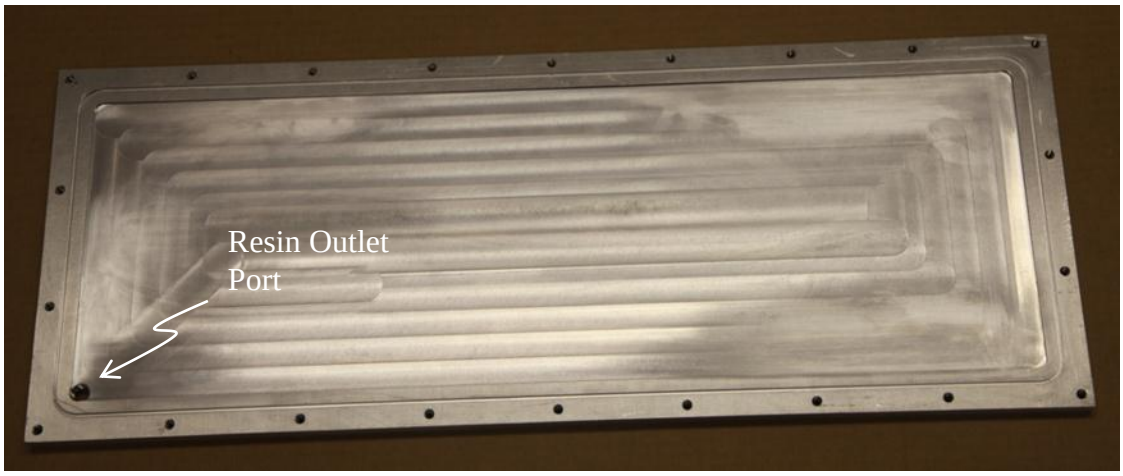

Figure 5. The inside of plate A.

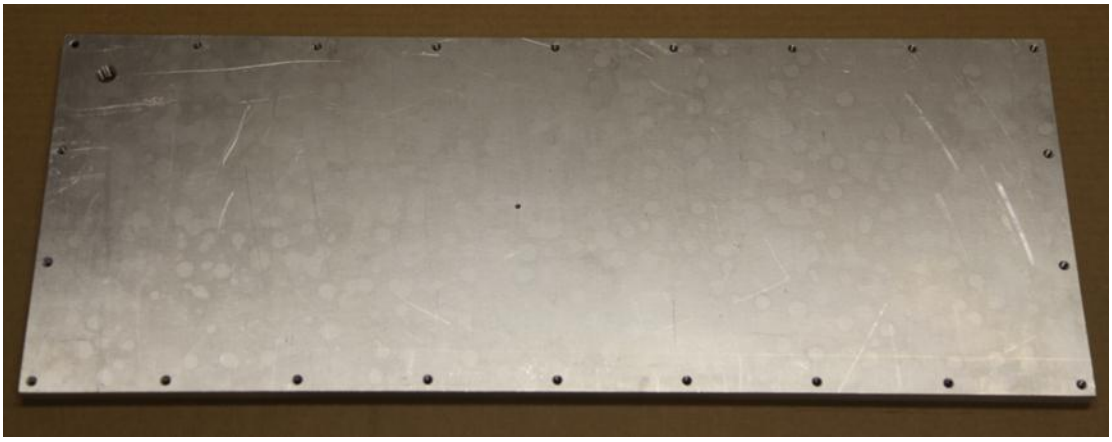

Figure 6. The outside of plate A.

The other plate (plate B) was flat on both sides. Plate B had the same outside dimensions as plate A (Figure 7). The outside of plate B had another ¼ in pipe tap thread hole for the resin entry. The resin outlet port (Figure 5) and the inlet port (see Figure 7) were at diagonally opposite ends of the assembled mold such that the inlet port was the bottom most point and the outlet port was the top most point of the mold. Plate B also had a recess machined on its side for a thermocouple attachment (see Figure 8). This thermocouple would monitor the heater temperature. There were additional holes drilled in plate B for help in the alignment of plates A and B and to help in separating the two plates after the part has been cured.

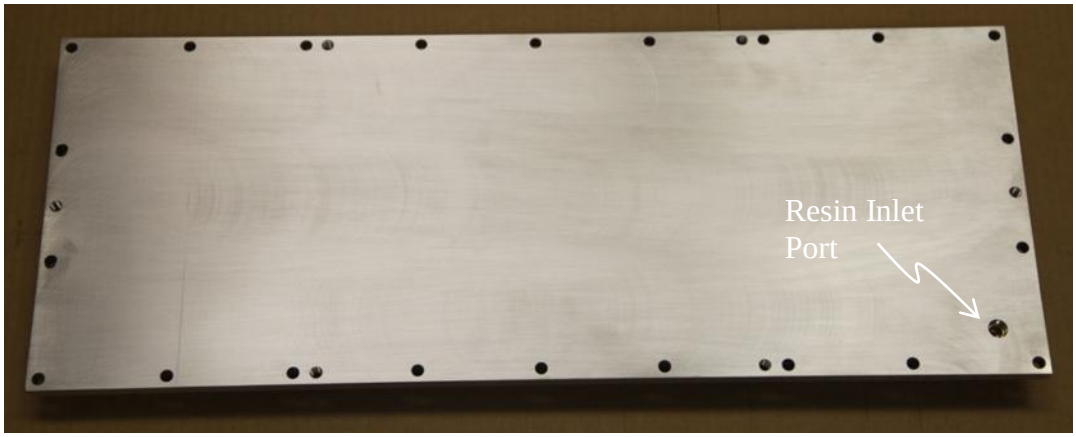

Figure 7. Outside of plate B.

Figure 8. Plate B.

Mold Preparation

Stacks of glass fabric samples were arranged over a nylon bleeder ply in a 2.2 mm deep rectangular cavity of one part of a two-part aluminum mold, Figure 9. To maintain the same final thickness of the three composite samples, each stack of 1581 and 7781 (thickness of one layer = 0.25 mm) contained 8 layers of cloth and the stack of 38050 (thickness of one layer = 1 mm) contained only 2 layers. The mold had a groove around the cavity to place an O-ring to provide a seal so that epoxy would not leak out of the mold during the resin impregnation process. The aluminum plate shown in Figure 9 also contained ¼ inch pipe tap threaded hole (hidden under the right most stack of 38050) machined at the top corner of the cavity for resin outlet port. The glass cloth samples were covered with another layer of nylon release ply (Figure 10). An O-ring was positioned in the machined groove and the other part of the mold (a rectangular aluminum plate, flat on both sides) was bolted tight to seal the glass samples between the mold plates, Figure 11. The top plate had a resin inlet port fitted with ¼ ID flexible hose (Kuri-Tec Polywire).

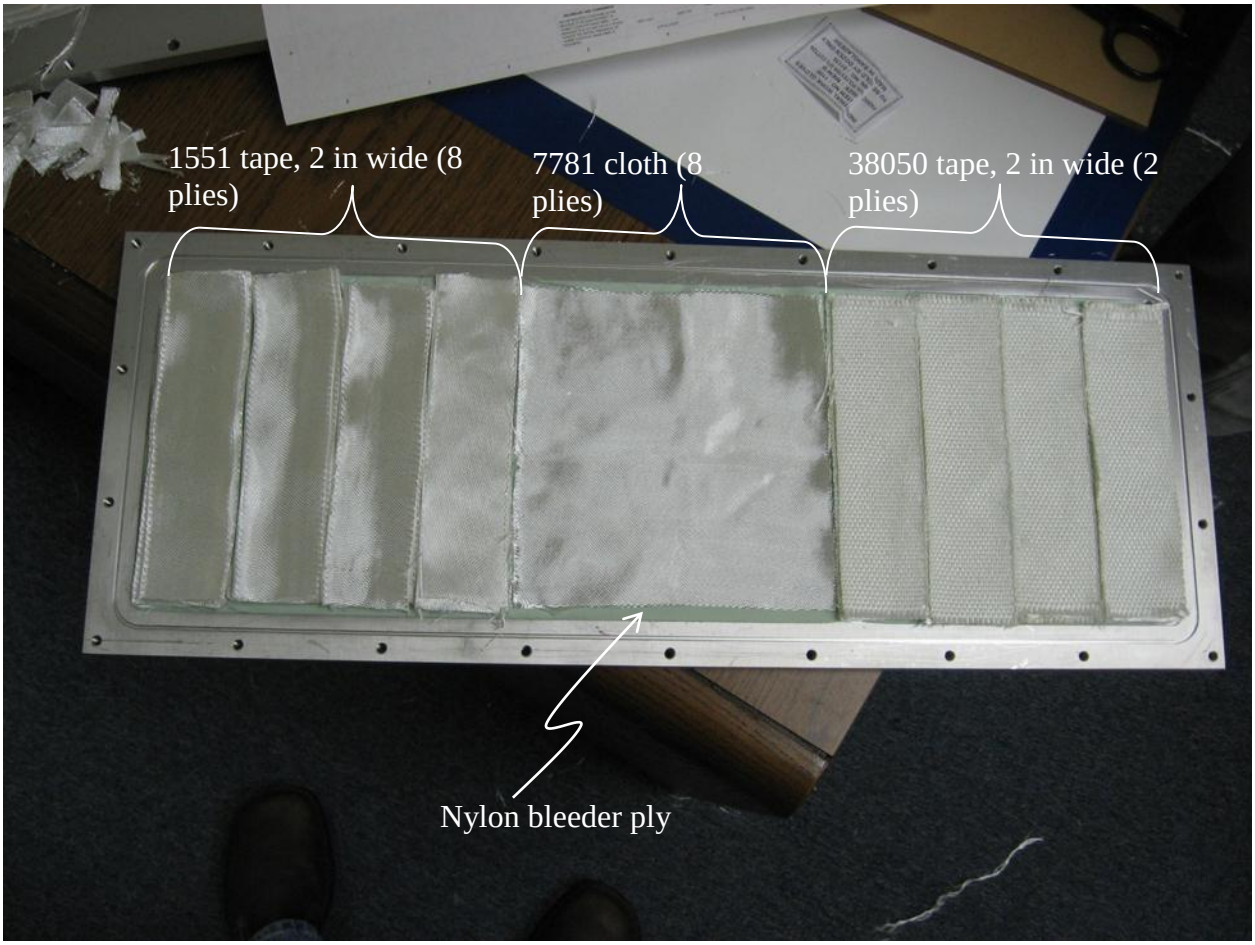

Figure 9. Glass Fabric arrangement on mold plate.

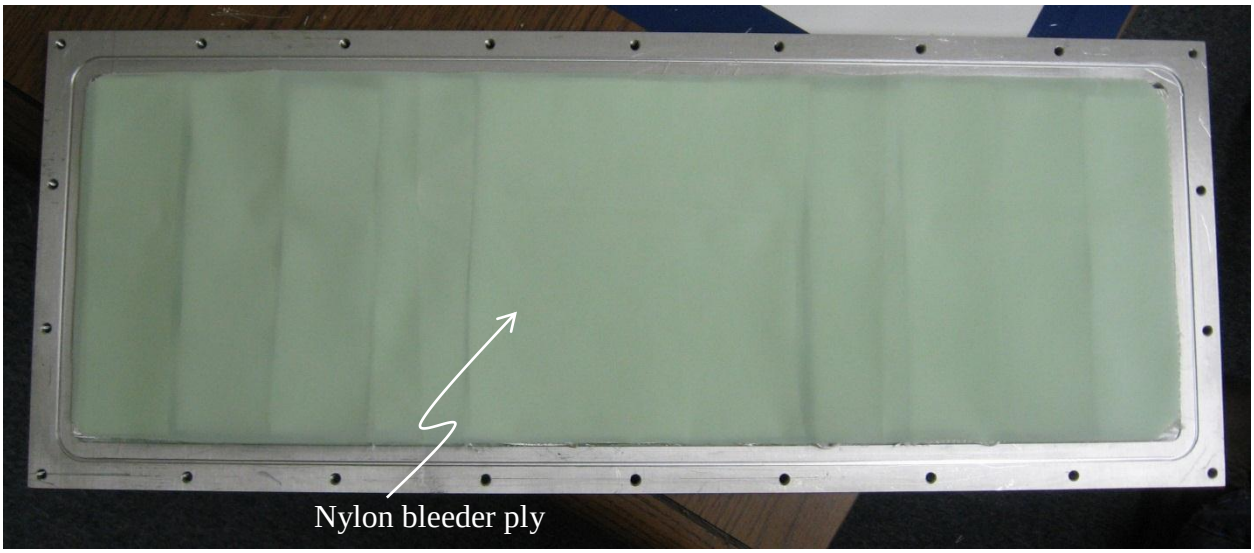

Figure 10. Glass cloths sandwiched between two nylon plies for easy release.

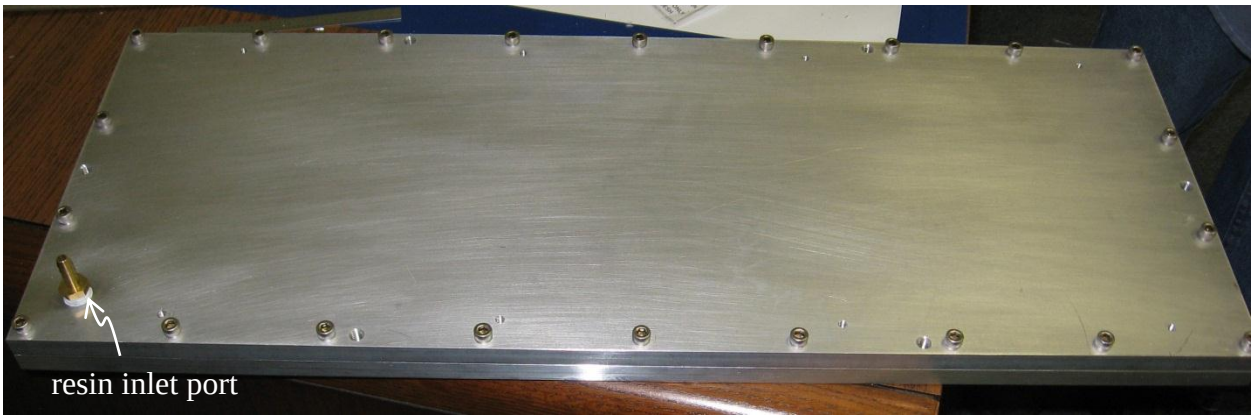

Figure 11. Mold plates containing glass cloths.

A 20 cm x 61 cm rectangular flexible silicone rubber fiberglass insulated heater (Omega SRFG-824, 100 volt, 480 W) was placed on top of the mold plate, Figure 12. The flexible heater was secured into position by bolting another flat plate on top of the heater, Figure 13. In order to monitor the sample temperature two thermocouples were attached – one located in the middle and outside of the mold plate with the rectangular cavity, and other one located on the side of the other mold plate, Figure 14. Tygon tubes were connected to inlet and outlet ports by means of compression fittings.

Figure 12. Mold plate with flexible heater placed on top.

Figure 13. Flat plate used to secure flexible heater.

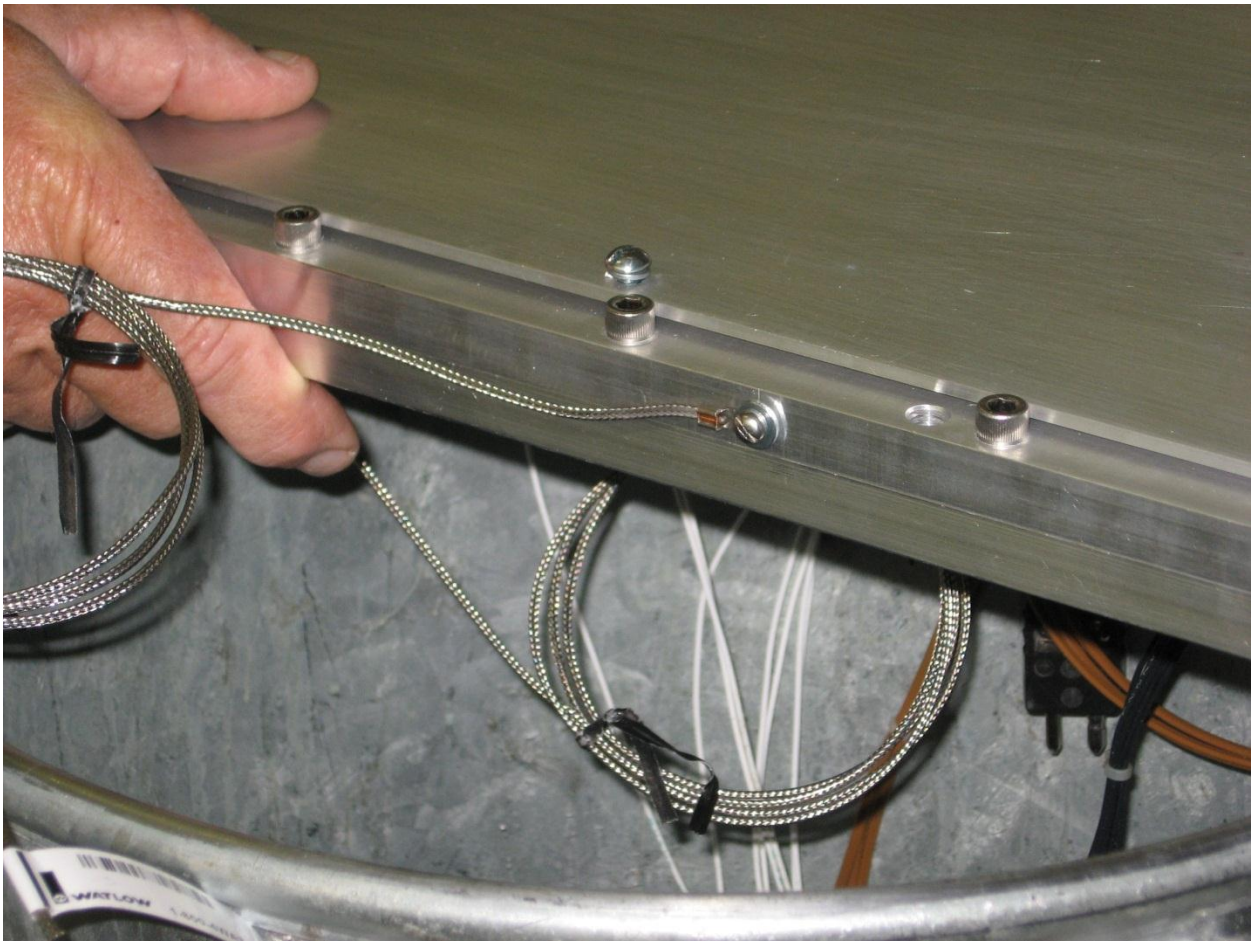

Figure 14. Thermocouple connected to side of mold plate.

Mold Tank

The mold tank was a cylindrical vessel 400 mm tall and 800 mm in diameter having a capacity of about 25 gallons. The mold was positioned in the middle of the mold tank, Figure 15. The mold tank was capable of sustaining a vacuum of less than 5 millitorr. A photograph of the sealed mold tank is shown in Figure 16. The mold tank was instrumented with several sealed ports accessible from the outside to connect a heater, thermocouples, vacuum pump, dry nitrogen, resin inlet port, and a view port, Figure 16.

After the mold was placed into the mold tank and all the instrumentation was connected and the mold tank lid was bolted tight.

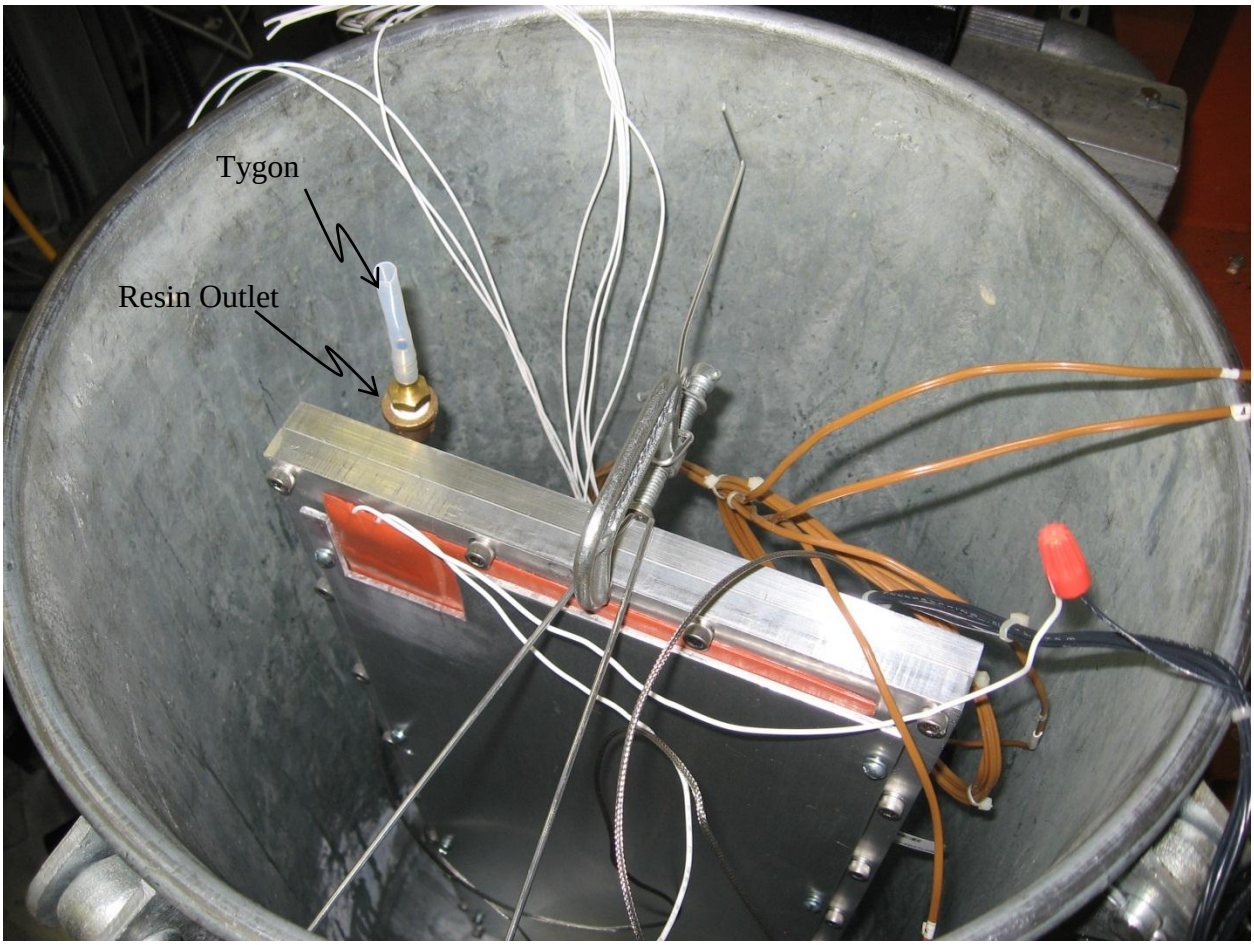

Figure 15. Positioning of sample mold in mold tank. The mold assembly was held in a vertical position.

Figure 16. Photograph of the sealed mold tank.

Sample Bakeout

In order to remove all moisture trapped inside the mold, it was heated to about 110°C and subjected to a vacuum of 100 millitorr. It was soaked at 110°C and 100 millitorr for about four hours. After the soak, the mold tank temperature was lowered to 50°C and the vacuum level was brought to about 1 torr and maintained at that level until the resin impregnation.

Resin Tank

The vessel used for the resin preparation was 1016 mm (40 inch) tall and 610 mm (24 inch) in diameter. Inside the vessel there was another cylindrical container that was 711 mm (28 inch) tall and 457 mm (18 inch) in diameter, Figure 17. This inner container is normally used for VPI jobs requiring about 25 gallons of resin. Since the volume of mixed resin required would be much smaller (not more than 1 gallon), another smaller container (resin tank) of height 381 mm (15 inch) and diameter 305 mm (12 inch) was used for resin mixing and heating. This resin tank was wrapped with two silicon rubber drum heaters (Type OMEGALUX SHDH698 120) having a wattage of 698W each. To minimize the heat loss from the drum heaters, they were tightly wrapped with several layers (approximately 3) of glass fiber insulation tape, see Figure 16.

Figure 17. Inner container where mixing of resin occurred.

About 1.5 gallons of resin mixed in the weight ratios given in Table 3 was poured into the resin tank, Figure 18. The main vessel is also capable of sustaining a vacuum in the millitorr range. The main vessel's lid was bolted tight and the plumbing for resin transfer from the resin tank to the mold tank was completed.

Figure 18. Tank containing premixed resin.

The resin tank was heated to 50°C and the resin was degassed at about 1.0 torr for approximately two hours. Initially during the degassing, bubbles were observed to appear rapidly (as viewed through the view port on the main vessel). As the degassing continued, the rate of bubbles decreased to almost no bubbles after two hours of degassing indicating that most of the air entrapped in the mixed resin had been removed. The resin was now ready to be transferred to the mold.

Resin Transfer Process

In order to transfer the resin from the resin tank to the mold tank, an adequate pressure differential between the resin and the mold tanks has to exist to allow the pump to move the resin. From previous experience, it was known that the required resin flow rate occurred when the resin tank pressure was at 1000 torr while the mold tank was at 1 torr. Therefore, the resin tank pressure was increased to about 1000 torr by allowing dry nitrogen into the tank. By controlling the pump speed the resin flow rate was set to transfer resin at a rate of 0.02 gallons/min. This rate was considered to be the rate that will allow a natural wicking of glass fibers. Mixed resin was allowed to enter the mold cavity until resin appeared in the tube attached to the outlet port. At this point, valve V4 was closed and the mold tank was pressurized to about 30 psi by allowing dry nitrogen into it. This step was necessary to ensure that any voids remaining in the mold cavity would be filled by the resin. If there were any voids, the application of pressure would produce a drop in the resin level in the tube attached to the outlet port. If there was a drop in the resin level, the dry nitrogen supply was stopped and the mold tank was again evacuated to a vacuum level of 1 torr. Valve V4 was opened and resin was again allowed to enter the mold to a point when resin appeared in the outlet tube. The pressure-vacuum cycle (called the milking process) was repeated until there was no drop in resin level in the outlet tube when the mold tank was subjected to 20 psi pressure. Such a condition would indicate that all the empty space in the mold cavity is filled with resin. At this point valve V4 was closed and the mold was again subjected to 30 psi pressure by introducing dry nitrogen into it. This pressure was maintained until resin cure was completed. The cure cycle began with an increase in oven temperature

from 50 °C to 90 °C (gel temp.) using rate of 10-15 °C/h. It was then held at 90 °C (+/- 5 C) gel temperature for 8 hours. The temperature was then increased to a cure temperature of 128 °C by ramping at rate of 10-15 °C/h. After being held for 12 hours at the cure temperature, the oven cooled to room temperature. The cure cycle can be seen in Figure 19.

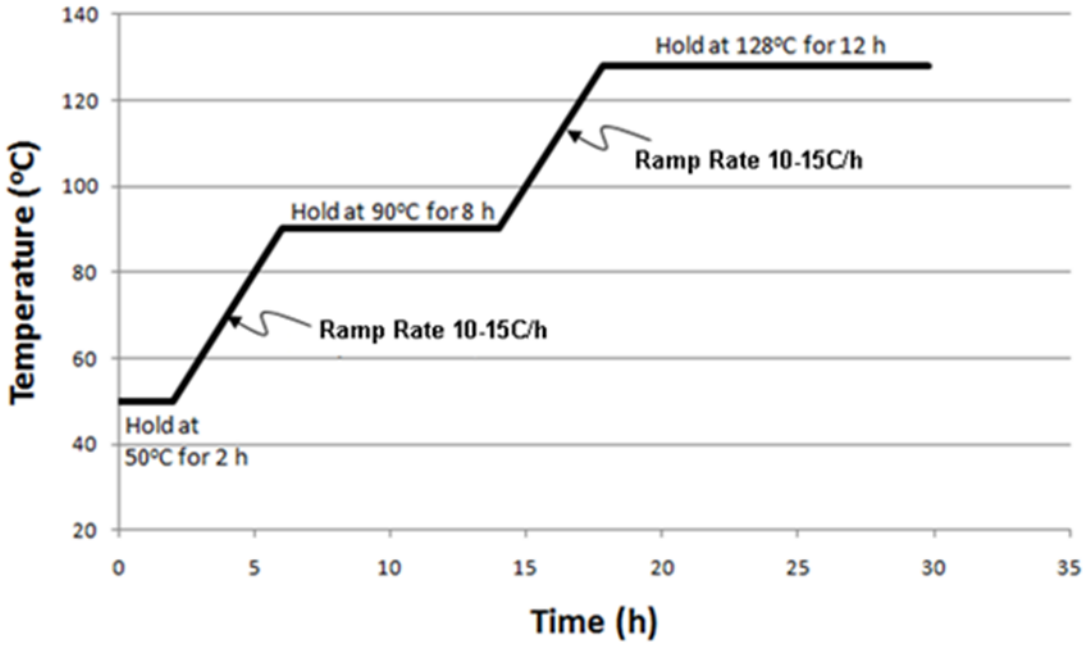

Figure 19. Cure cycle used in the completion of the composite samples.

Composite Samples

After the completion of the cure cycle, the heater was turned off and the mold was allowed to cool. The three types of composite plates were removed from the mold cavity (Figure 20). The average thickness of the three types of composite plates was 2.15 mm. A diamond-coated wheel cutter was used to cut rectangular samples for 3-point bend testing that were 55 mm long and 6.2 mm wide (see Figure 21). The span length (S in Figure 22) was 45 mm to provide an S/t ratio of about 20. However, it is necessary to note that about ¾ of the 1581 laminate plates were cut to a sample length of 45 mm before the mistake was caught. The samples were cut in a way such that the sample's lengths were parallel to the warp direction of the weave pattern. With plain weave patterns (such as in 38050), both directions have the same pattern, but with 8-harness satin weaves the properties are different in warp and fill directions.

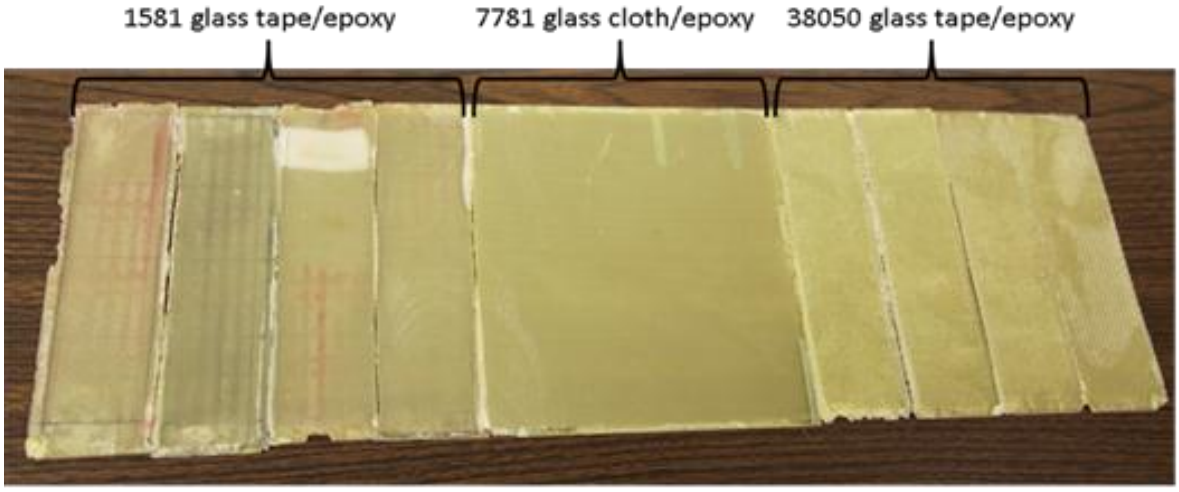

Figure 20. The three types of composite plates fabricated using the VPI process.

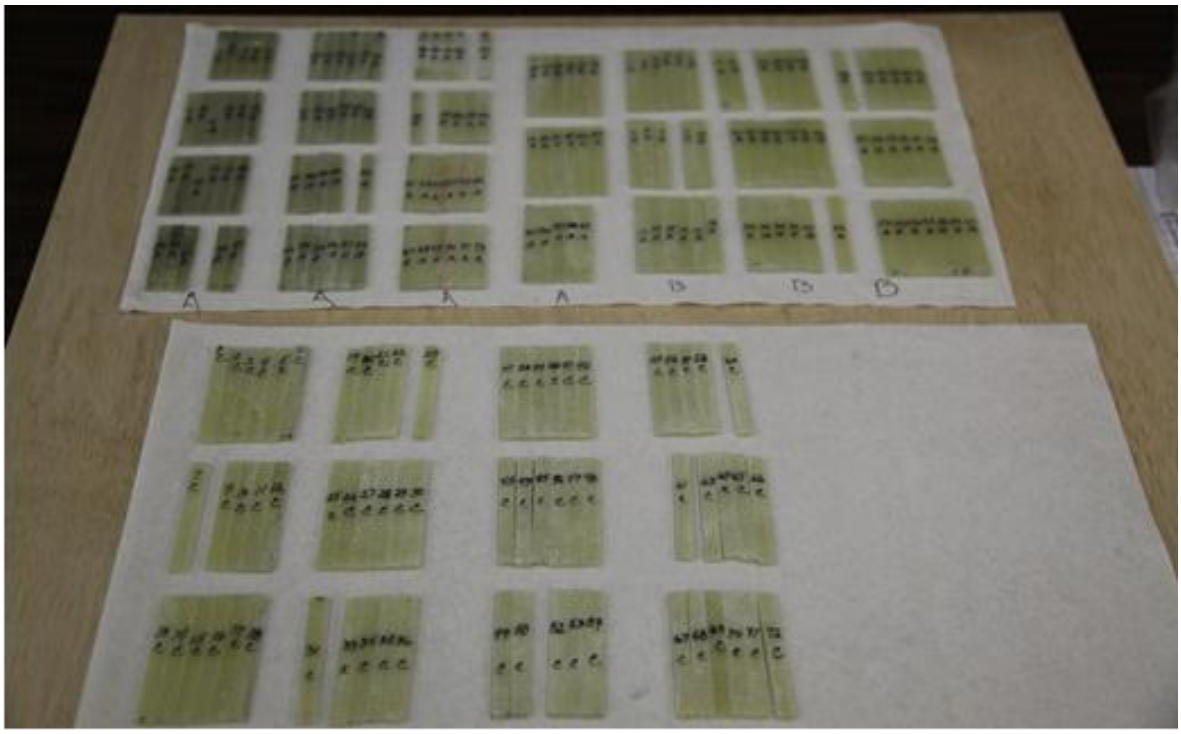

Figure 21. 3-point flexure specimens were cut from the composite plates.

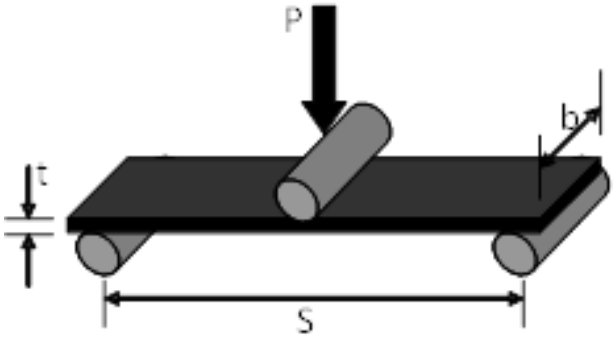

Figure 22. Schematic of flexure test.

Densities, Fiber and Void Volume Fractions

Densities

Densities of the laminate samples from each type of glass were measured by measuring the mass of rectangular samples of known dimensions (seen in Figure 21). Five random samples were taken from each of the three different fiberglass samples. The mass of each individual laminate sample was divided by that sample's measured volume. The density of cured samples of neat epoxy was also measured the same way.

Fiber and Void Volume Fractions

Using the measured densities of composite laminates and epoxy and assuming zero voids, the fiber volume fractions of the composite laminates were calculated from the rule-of-mixture equation,

$$\boldsymbol{\rho_l = (x) * \rho_f + (1 - x) * \rho_e} \ldots\ldots\ldots\ldots\ldots\ldots\ldots\ldots \textit{(1)}$$

where ρ_l is the laminate density, ρ_f is the glass fiber density, and ρ_e is the neat epoxy density.

The composite laminates were assumed to be void-free because prior to the VPI process, the mixed epoxy was degassed for 2 hours at 130 Pa and at 50°C.

3-Point-Flexure Tests

The 3-point-flexure tests were completed at both room temperature (295K) as well as at liquid nitrogen temperature (77K). This was done in order to not only compare the behavior of the laminates with each other, but also to see how the laminate behavior changed at low temperatures. A modified version of ASTM Standard D 790 procedure

A was followed [21]. The modification was due to the radii of supports and the loading noses differing being less than 5 mm.

Flexure Apparatus

Since the testing had to be completed at the two different temperatures, it was necessary to use an apparatus that could accommodate the tests at both room temperature and liquid nitrogen temperature so that the data could be easily compared. Due to the cost of this type of apparatus, one was constructed in house. There were many different attempts before coming to a final design that suited the needs of the tests to be completed. Issues encountered included:

1. Load could not be added to the load carrying rod in large increments. It was determined after looking at the noisy data collected that the weights needed to be added in small quantity increments due to the minimal amount of deflection the sample could withstand before failure.
2. Due to the small amount of deflection of the samples during the loading, the machine vibration had to be kept to a minimum. At first, the linear variable differential transformer (LVDT) was positioned so that it measured the displacement of the plate at the top of the load bearing rod where the load was added. This created very noisy data due to the movement at the top of the rod being considerably higher than what the sample was experiencing at the bottom of the rod. This was mostly caused by the length of the rod and there were no stabilizing support beams to help reduce the movement.

3. Submerging the sample under liquid nitrogen without freezing the test apparatus. It order to test the laminate samples at liquid nitrogen temperature, it was necessary to have them completely submerged under liquid nitrogen throughout the test. However, it was found that submerging the lower portion of the bending fixture in liquid nitrogen caused frozen frost build up around the apparatus itself and there was no longer free movement of the load bearing rod through the ball bearings used to help stabilize the rod. This caused the data to be skewed and unusable.

After some trial and error tests to help overcome these issues, a final design for the machine was developed and can be seen in Figure 23. The issues stated above were resolved by using small lead pellets for the load, securing a stable tab close to the bottom of the rod for the Omega LD621-100 LVDT to take deflection measurements from, and by using a reservoir machined from G-10 composite laminate to contain the liquid nitrogen. The sample loading was done inside the reservoir made of G-10 material. This material was chosen because it is quite rigid and also a good insulator so the liquid nitrogen would not evaporate quickly during the sample loading. The end supports of the sample were smooth 6.33 mm diameter steel cylindrical pins. The sample loading was achieved using a 12.7 mm diameter steel rod that had its loading end machined to a radius of 2.5 mm cylindrical surface. In these tests a large span-to-thickness ratio (S/t) of 20.36 (S=45 mm, t=2.21 mm) was used and the flexural elastic modulus and strength of each type of laminate were measured. An Omega LCR 250

load cell was used to record the load on the sample at a given time. Personal DaqView XL software was used to record the data collected by the load cell and LVDT through Microsoft Excel.

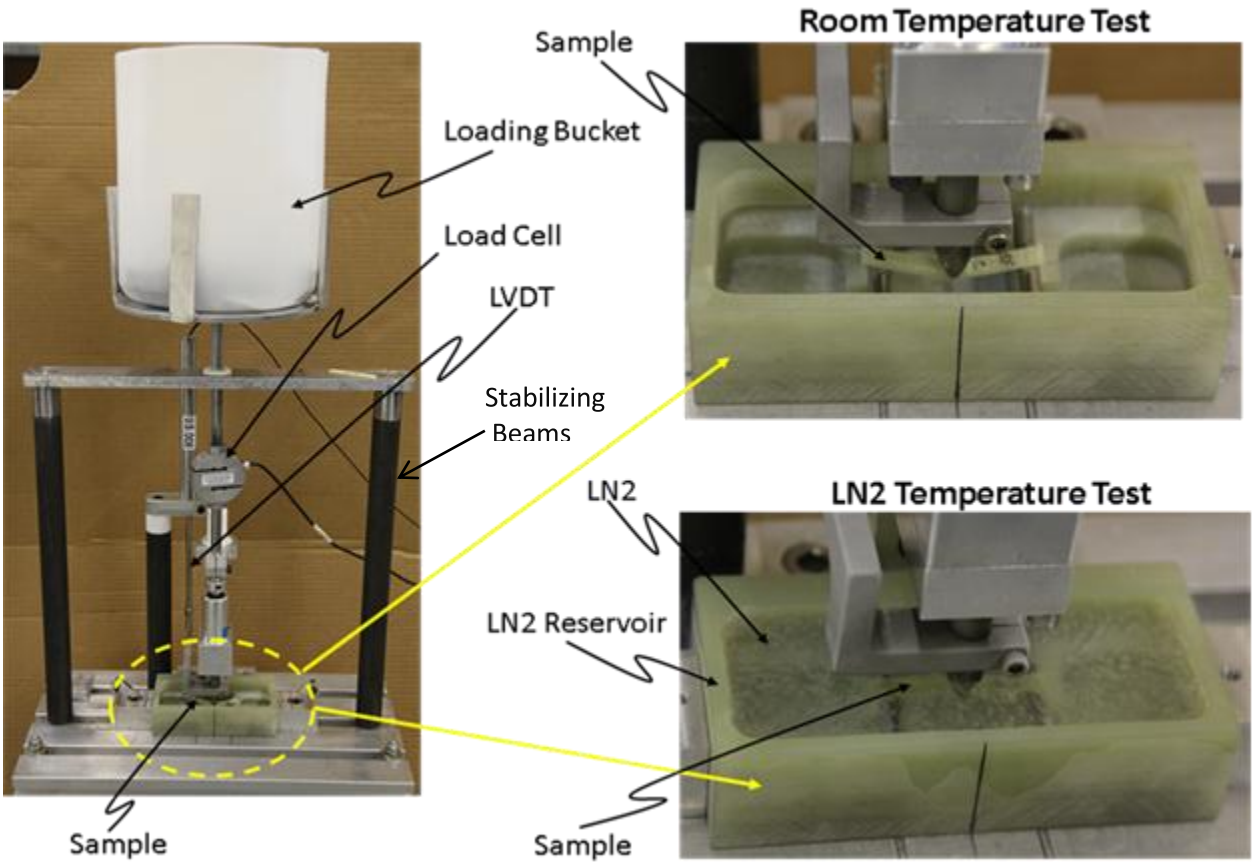

Figure 23. Picture of the apparatus used for the 3-point-flexure tests. A closer view of the sample during testing at both temperatures can be seen.

Experimental Method at Room Temperature (295K)

The 3-point bend tests were first completed at room temperature. Eight samples were chosen at random from each of the three composite laminates, except in the case of the 1581/epoxy laminate where 10 samples were chosen: five from the 45 mm samples and 5 from the 55 mm samples. A sample was placed so that its center was positioned at the tip of the load bearing rod, seen in Figure 22. The load was applied by adding weights to a plastic bucket at a rate of about 200 g per second until failure. It is important to note that this method of loading was preferred since the maximum failure loads in the composites were less than 60 kg. This method provided a cleaner noise-free data (compared to that obtained with servo-hydraulic machines at low load ranges). The sample load and midpoint deflection were measured by a load cell (load capacity = 1100 N) and an LVDT, respectively. This process was repeated for each of the samples tested at room temperature.

Experimental Method at Liquid Nitrogen Temperature (77K)

Again, eight samples were chosen at random from each of the three composite laminates, with the exception of the 1581/epoxy laminate. Prior to applying any load, the samples were submerged in liquid nitrogen for about ten minutes to provide temperature equilibrium. The process that was utilized for the room temperature samples was then applied to these samples until all the samples had failed. During the loading, the liquid nitrogen level was always maintained to the top of the reservoir so that at all times the sample was completely immersed.

Fractography

Representative photographs of failed samples from each of the three laminates at both temperatures were taken using a high definition Canon camera. These photographs were taken to get an initial optical evaluation of the failure of the samples. After the initial evaluation was complete, the samples were placed in an LEO 1525 Field Emission SEM with an Oxford EDS Link X-ray system to get a closer look at individual fibers in order to see how the fiber/epoxy adhesion faired after sample failure. Prior to being imaged in the SEM, the samples were coated in a layer of gold in order to reduce charging of the samples.

Constant Load Flexural Creep Tests

Preliminary stages of creep data collection were completed in order to compare the time-dependent behavior of the three different composite laminates at room temperature. Due to time restraints, the in depth study that would provide the amount of data needed to model the time-dependent behavior of the laminates used was not able to be completed at the time this thesis was completed. Future work is recommended that would include creep testing at liquid nitrogen temperatures as well.

Flexural Creep Apparatus

The same apparatus that was utilized in the flexure tests was again used for the creep tests and can be seen in Figure 23.

Experimental Method

Flexure creep tests were desired for this study to compare how the three different laminates responded to a constant stress over a length of time. The short-term flexural properties were evaluated and compared through 3-point flexure tests and flexure creep tests were used to evaluate and compare the properties for a longer term. Due to time constraints, tests were run for a maximum of ten days if the sample did not fail before then. Samples were again chosen at random in order to be placed under a constant load to see how the deflection would change with time. The test procedure closely followed ASTM Standard D2990 [21].Each sample was placed on the support rods, just as in the case of the flexure tests, and then the load was applied at the same rate as before until the desired load for the creep was reached. Each laminate type was tested at three different loads. The creep load was chosen to be approximately 60-65% of the failure load for the first run for each of the samples. It was then increased or decreased, depending on whether or not that sample failed during the test, to determine the remaining two creep loads. Each laminate type had three samples for each load to obtain statistically relevant data, with the exception of the 1581/epoxy laminate due to time restraints. Data for each sample was collected until the sample failed or for no more than ten days.

CHAPTER IV
RESULTS AND DISCUSSION

Densities and Fiber Volume Fractions

The measured laminate and epoxy densities and the calculated glass fiber volume fractions are shown in Table 3. The laminate densities vary because to achieve equal thickness and equivalent applied pressure during the VPI process, the number of glass cloth plies was varied dependent on the thickness of the glass weave. The density of E-glass fibers given by the manufacturer was 2.54 g/cm^3.

Table 3. Densities and Fiber Volume Fractions of Laminates

	7781/epoxy	1581/epoxy	38050/epoxy	Epoxy
Density (g/cm^3) (measured)	1.81	1.71	1.56	1.22
Fiber Volume Fraction (%)	44.6	33.3	25.8	-

3-Point Flexure Tests

Representative load-displacement plots for the three types of laminates at 77K and 295K are shown in Figure 24.

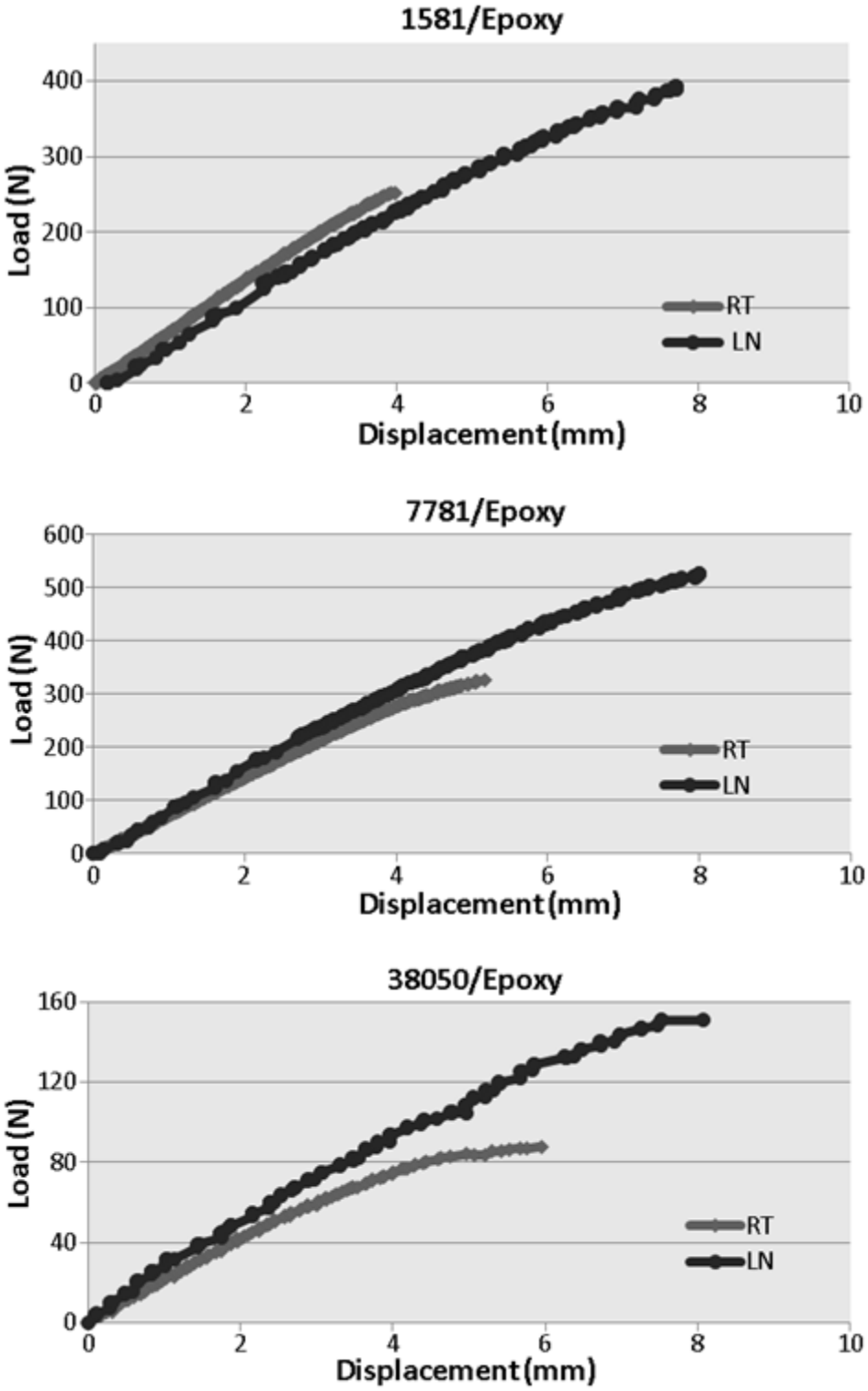

Figure 24. Representative load-displacement plots at room and liquid nitrogen temperatures for the three types of glass/epoxy composites.

Using the standard beam- bending equations, the flexural elastic modulus, flexural strength, and maximum flexural strain can be calculated from the following equations.

$$Flexural\ Elastic\ Modulus = \frac{S^3(slope\ of\ load - displacement\ curve)}{4bt^3} \quad \text{..... (2)}$$

$$Flexural\ Strength = \frac{3P_{max}S}{2bt^2} \quad \text{..... (3)}$$

$$Maximum\ Flexural\ Strain = \frac{6\delta_{max}t}{S^2} \quad \text{..... (4)}$$

where S, t, and b are defined in Figure 22, and P_{max} and δ_{max} are the maximum load achieved and the corresponding mid-point deflection, respectively.

The individual flexural elastic moduli and strengths for all the samples are shown in Figure 25 and Figure 26, respectively. Figure 27 shows the comparisons among the three types of composites for their average flexural elastic modulus, average flexural strength, and average maximum flexural strain at 295K and 77K. Data for a sample of neat epoxy was obtained from another graduate student working with the same resin.

(a)

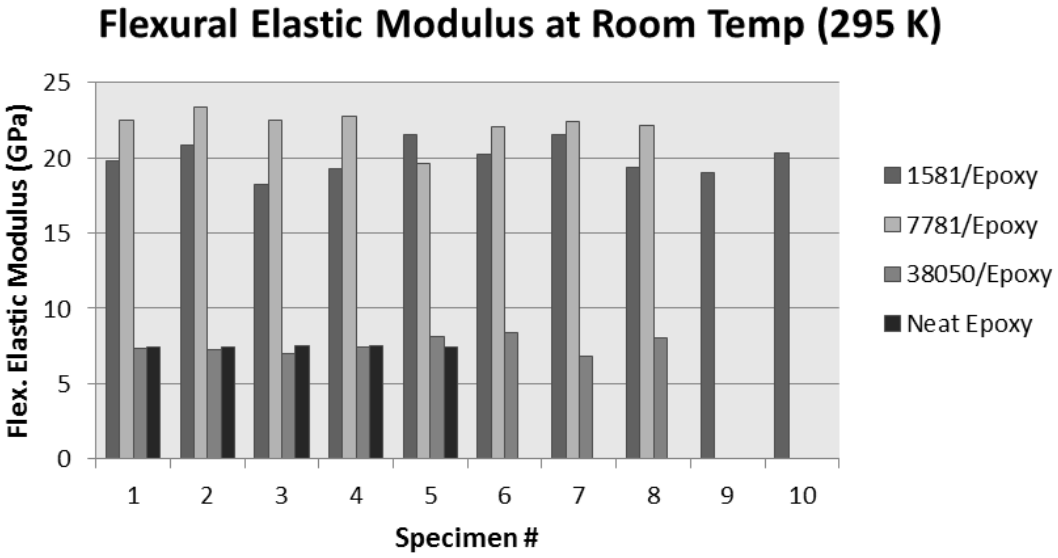

(b)

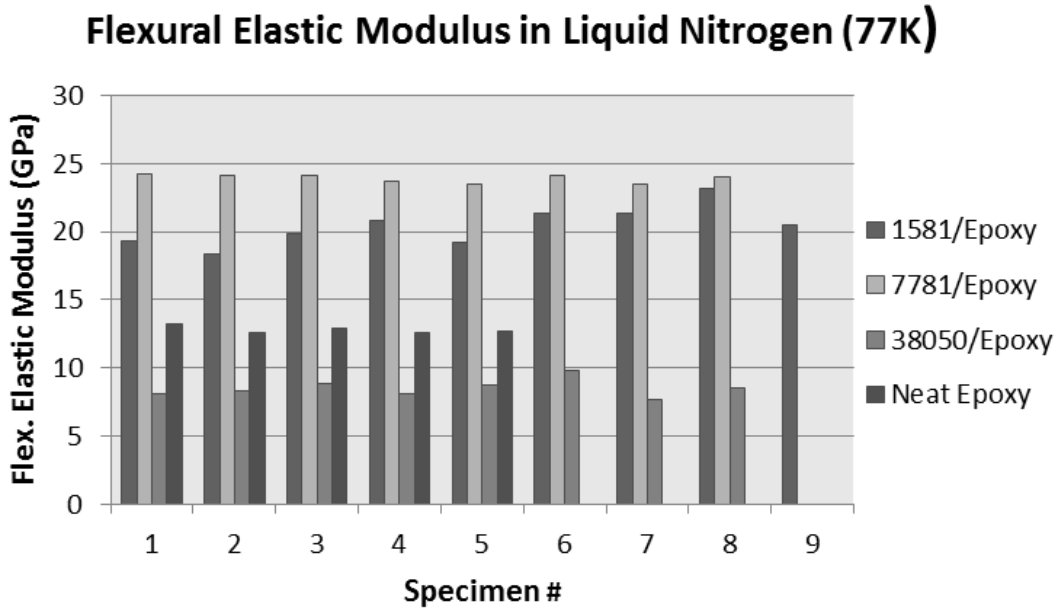

Figure 25. Individual flexural elastic modulus values for the three types of glass/epoxy composites as well as the neat epoxy at a) 295K and b) 77K.

(a)

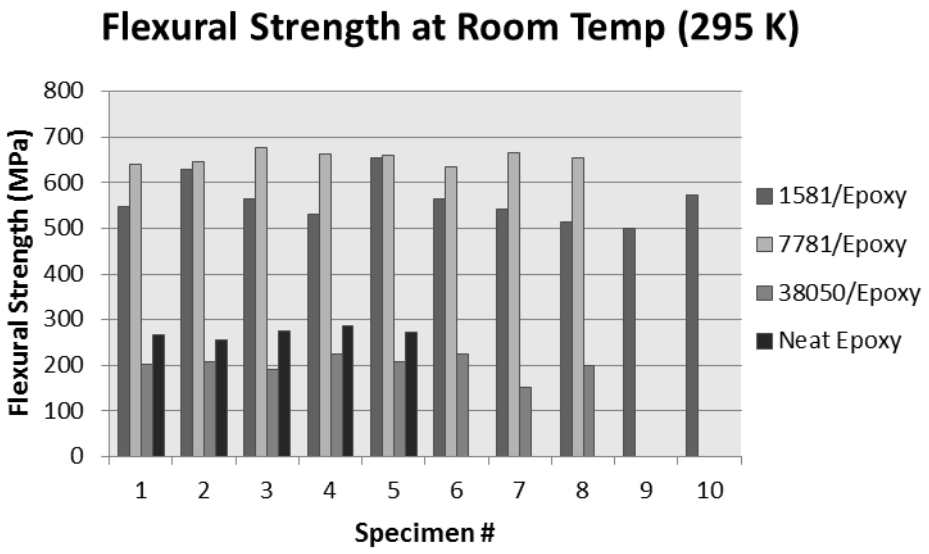

(b)

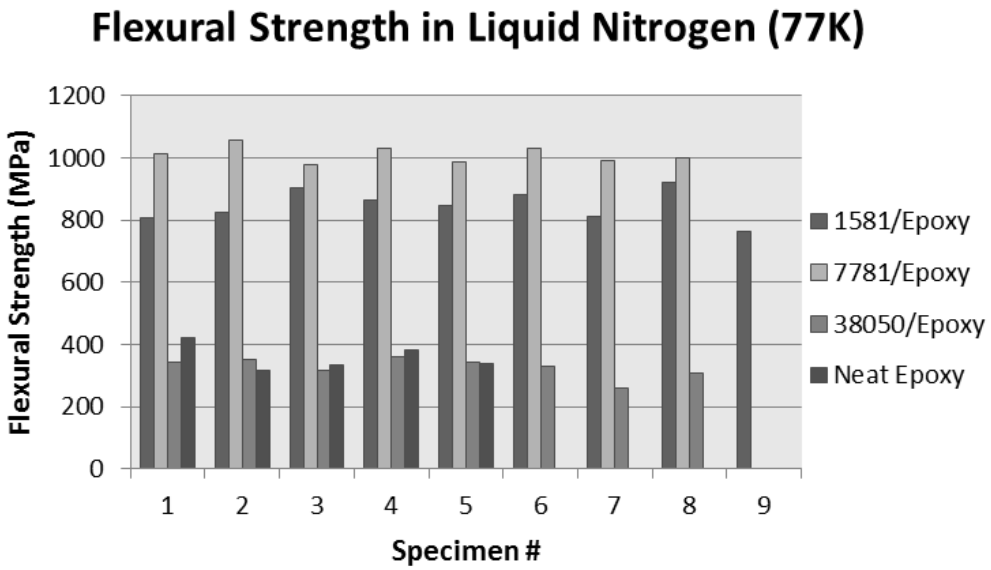

Figure 26. Individual flexural strength values for the three types of glass/epoxy composites as well as neat epoxy at a) 295K and b) 77K.

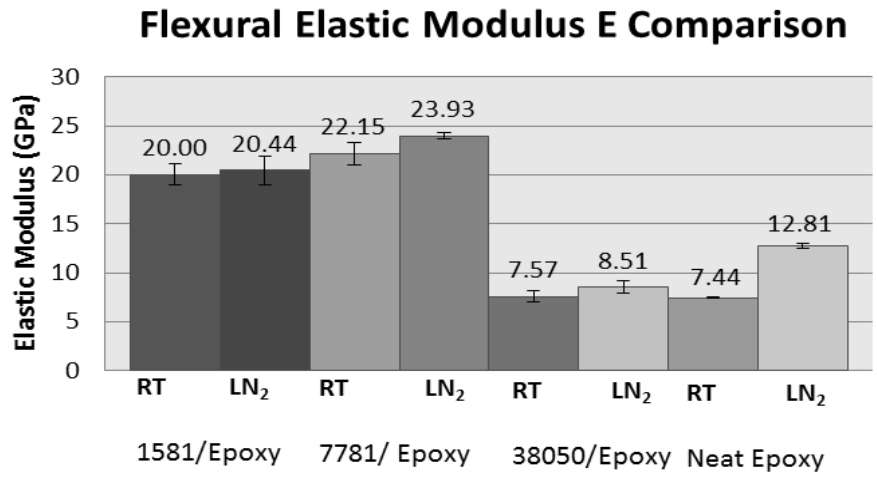

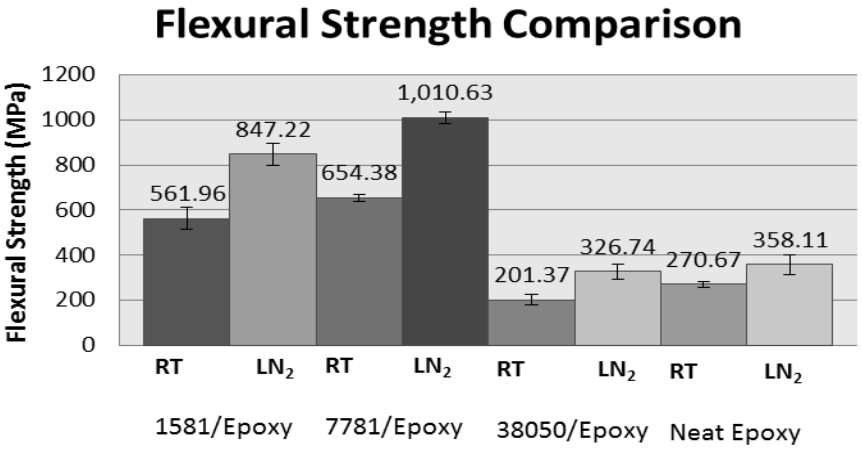

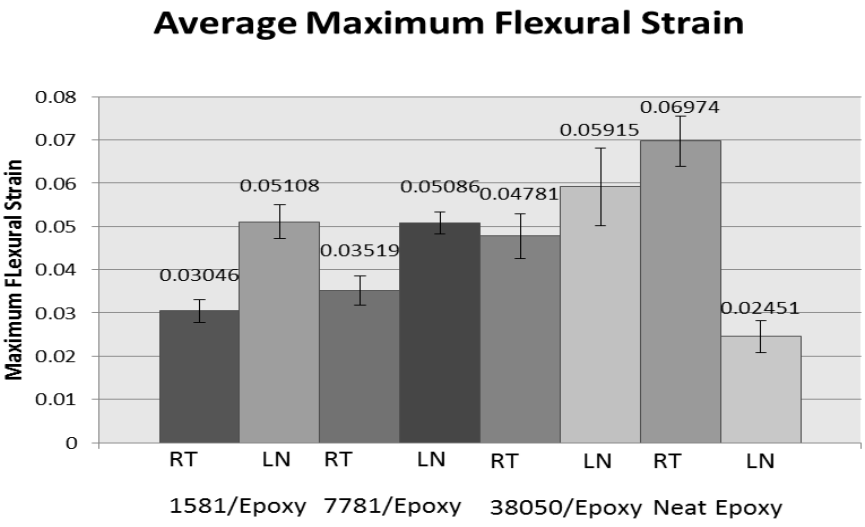

Figure 27. Comparison of flexural elastic modulus, strength and maximum strain at the two temperatures for the three types of glass/epoxy composites as well as the neat epoxy.

The key observations from these charts are as follows:

(i) The data scatter is low, i.e. the results are reproducible

(ii) The 7781/epoxy was the strongest and stiffest. The 38050 performed quite poorly compared to both 7781 and 1581. The poor performance of 38050/epoxy can be attributed to the low areal density of both 38050 glass tape and the density of 38050/epoxy composites.

(iii) While there is only a modest increase (about 5 to 10%) in the flexural elastic modulus from room to liquid nitrogen temperatures, the flexural strength increases by more than 50% for the three glass/epoxy composites. The low dependence on temperature of the former may suggest that the flexural elastic modulus is primarily dependent on glass content; the elastic modulus of glass fiber increase only by about 10% from 295 to 4 K [23]. But, the stronger temperature dependence of the bend strength suggests that the resin may also play a role; epoxy resins increase in tensile strength by 50-75% from 295 to 77 and 4K [23]. This increase can also be seen in the neat epoxy sample.

(iv) The maximum strain was largest for 38050/epoxy followed by 7781/epoxy and 1581/epoxy at both temperatures.

(v) The failure strain also increases for all three composites at lower temperature which was expected because the flexural strength increases but the flexural elastic modulus does not increase at low temperature.

(vi) The 38050/ epoxy sample had a strength and stiffness similar to the neat epoxy sample. This shows that the 38050 fiber gave no added benefit to the properties being evaluated in this study.

Plotting the flexural strength and flexural elastic modulus data as a function of composite's density shows almost a linear relationship in both flexural elastic modulus and strength at both test temperatures (295 and 77K), Figure 9.

(a)

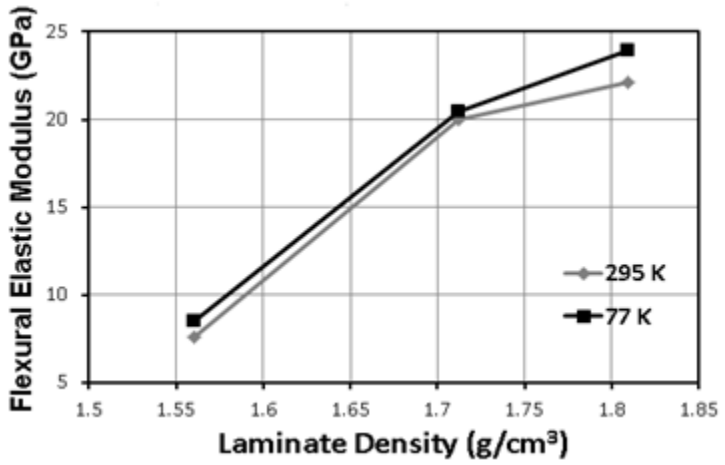

(b)

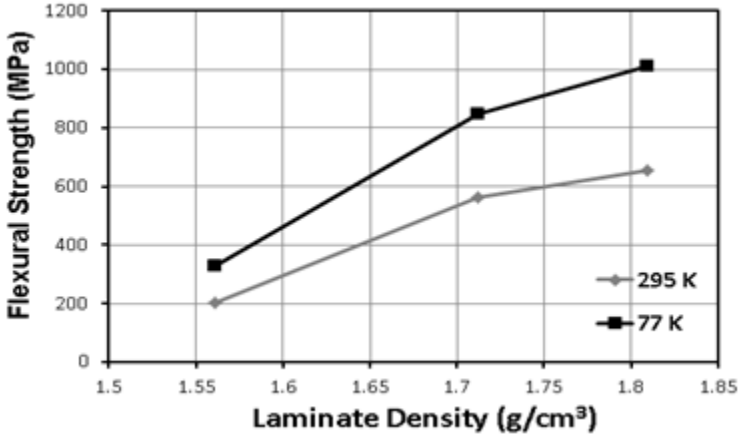

(c)

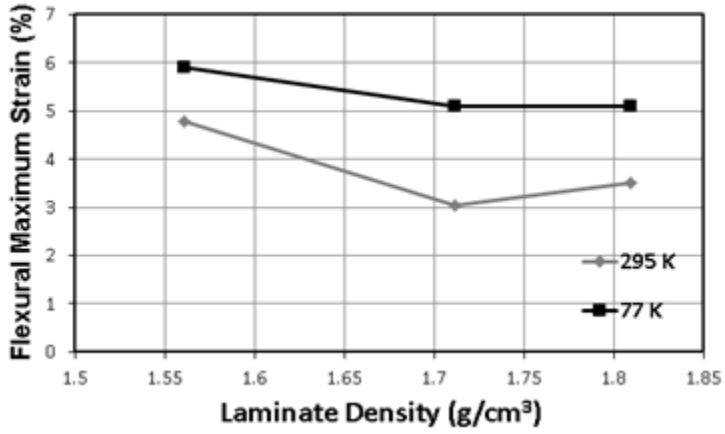

Figure 28. Correlation of laminate flexural properties with its density.

In the absence of significant void content, the density of the composites is dependent on their ratio of glass-to-resin; higher glass contents result in higher densities. Higher glass contents are achieved through the use of glass cloths or tapes that have higher densities, if their fabrication pressures during resin transfer and cure remain constant. The linearity of both the flexural strength and flexural elastic modulus at both temperatures indicates that both properties are dominantly dependent on laminate density, thus on glass content.

Fractography

Optical Photographs

Photographs of representative failed samples are shown in Figure 29-Figure 32. Types 7781 and 1581 show similar failure modes: interlaminar delaminations along the tensile side of the specimens, followed by resin cracking/fiber breakage along the tensile side of the specimens. Both types also had limited transverse cracking in the region of the specimens farther out from the central point of loading and delamination areas. The length of the delamination along the specimen length was slightly longer for type 1581, compared to 7781, at both test temperatures. More bending and more localized delamination were observed in the specimens tested at room temperature, compared to 77 K. The compression side of both 7781 and 1581 specimens never failed and interlaminar delaminations were much less frequent in this area.

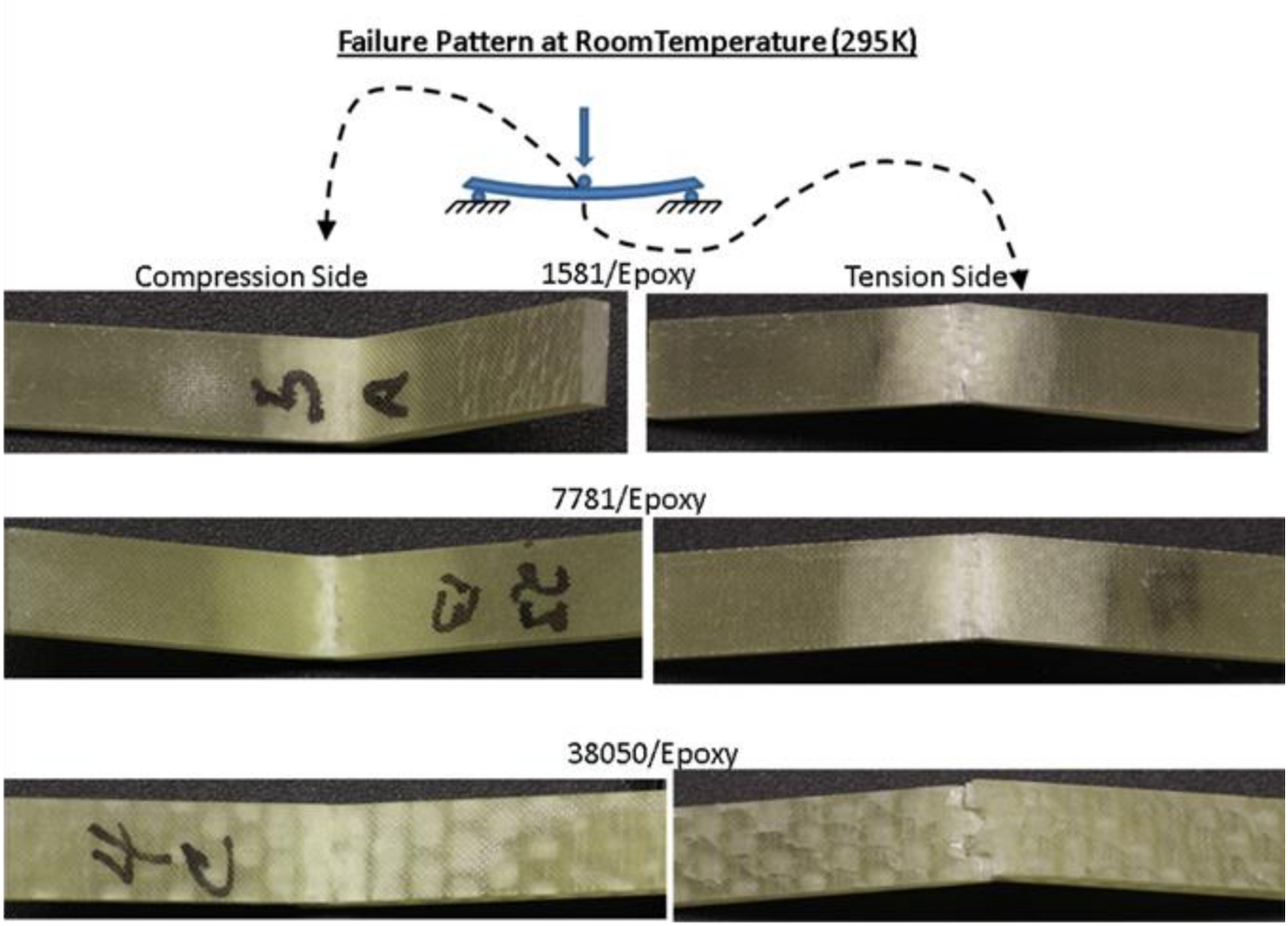

Figure 29. Photographs of the failed samples' middle sections tested at 295K showing the failure pattern on tensile and compressive sides.

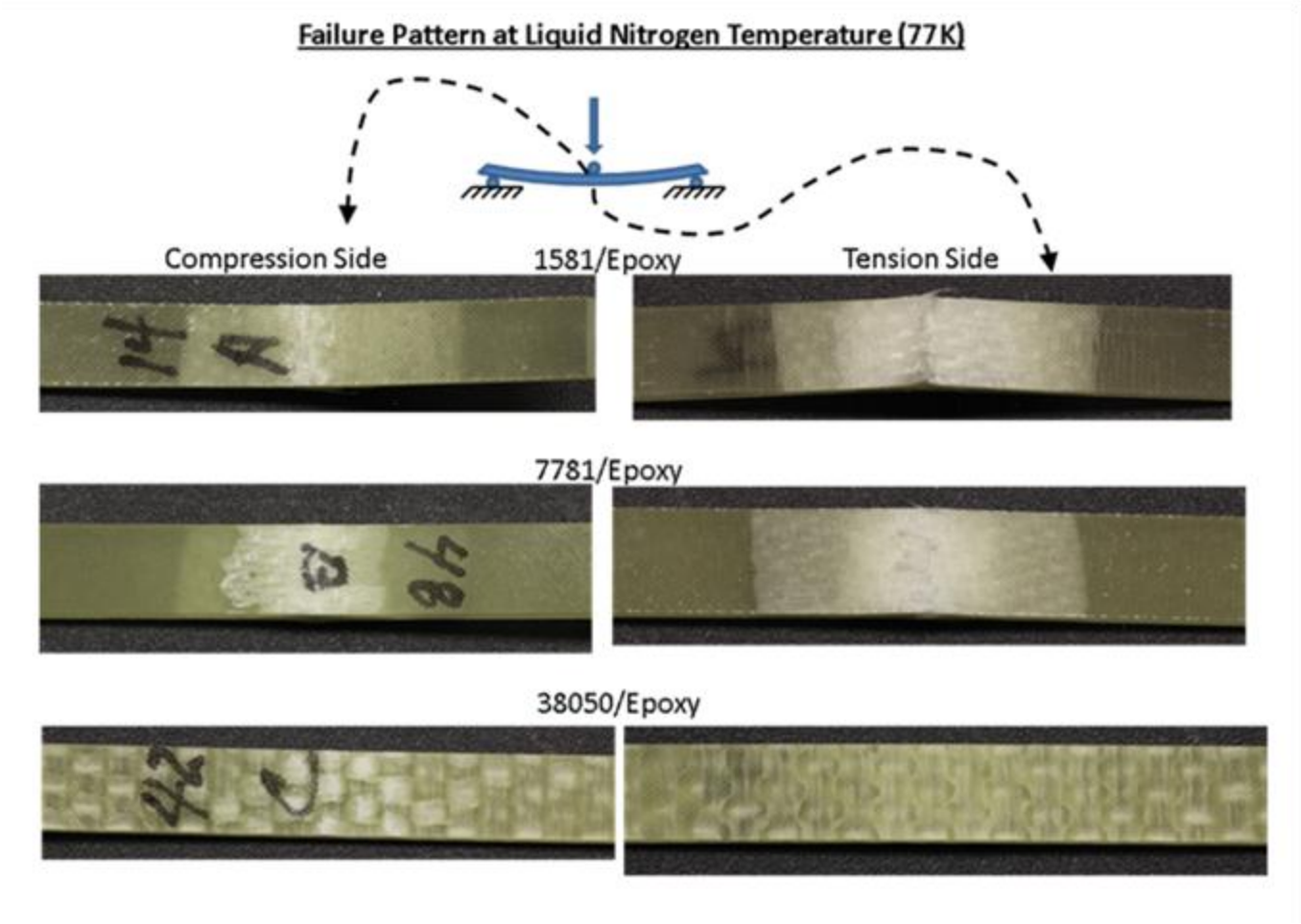

Figure 30. Photographs of the failed samples' middle sections tested at 77K showing the failure pattern on tensile and compressive sides.

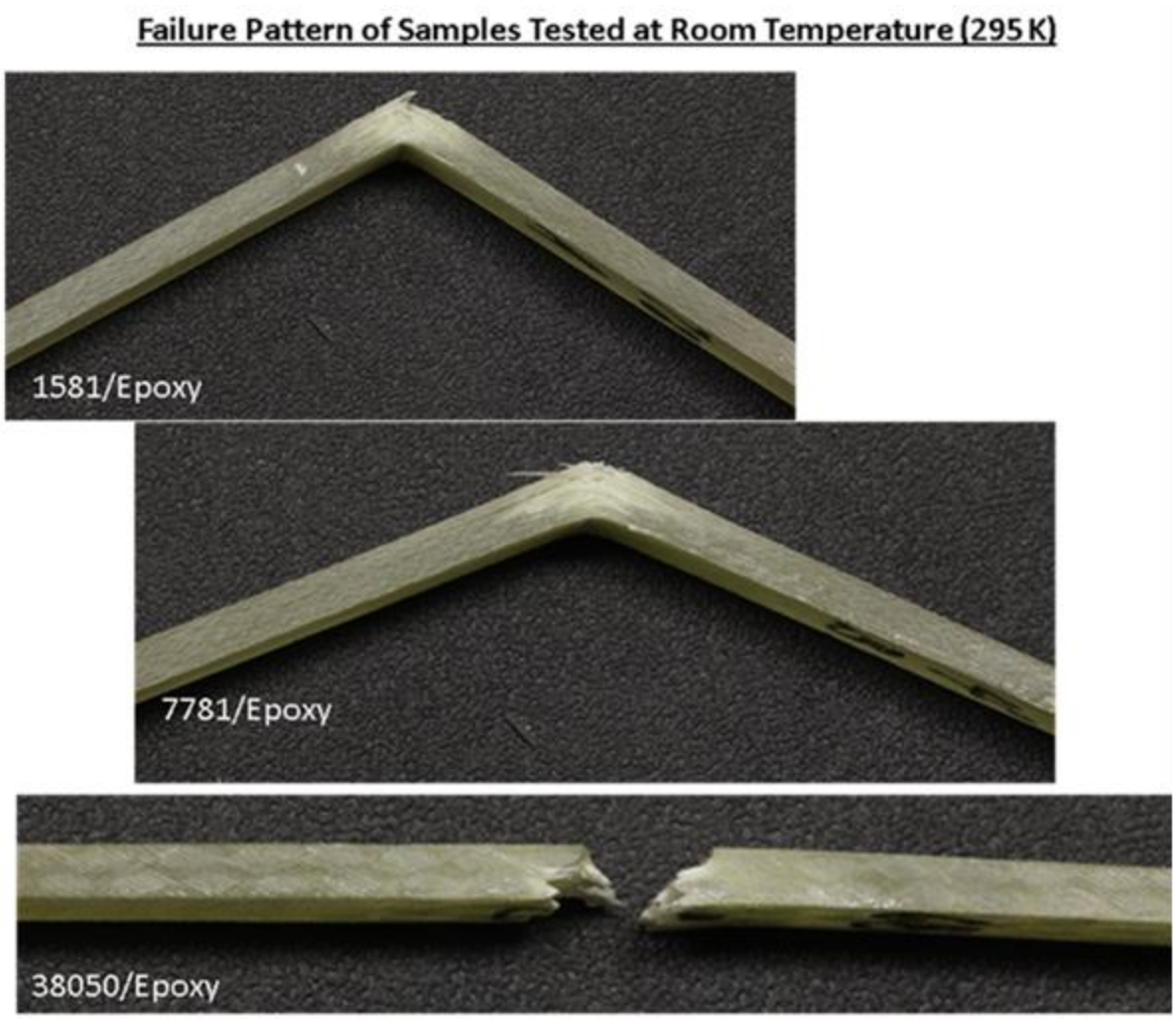

Figure 31. Photographs of the side view of the failed samples' middle sections tested at 295K showing the failure pattern.

Figure 32. Photographs of the side view of the failed samples' middle sections tested at 77K showing the failure pattern.

In contrast, type 38050 specimens fractured completely. The fractures were brittle, perpendicular to the plane of the specimen and parallel to the loading direction. No specimen bending and limited delaminations were observed. Macro-dimensional, interior cracking along the entire length of these specimens was present. Localized debonding was also observed, indicating a lack of bond strength between the glass fibers and resin. This was not observed in the 1581 and 7781 specimens.

The extended length of discoloration (white region in the middle of samples in Figure 29 and Figure 30) in 1581 and 7781 samples is indicative of good fiber/matrix bonding.

In these samples, the length of discoloration increases at 77K, which may suggest improvement in bond strength at lower temperature. A plausible explanation for this phenomenon may be due to the material shrinkage during cooling. Epoxy resins have higher thermal expansion coefficient than glass (from 295-4K epoxy resins contract about 1.2%, E-glass fibers about 0.1%) [15]. Due to the difference in the thermal expansion coefficient, two possible mechanisms may exist when the composite temperature is lowered, Figure 33. When a fiber is surrounded by a matrix, the shrinkage would produce compressive stresses on the fiber, Figure 33a, which in turn, have an effect of increased interfacial shear strength between the fiber and matrix. However, a pocket of matrix surrounded by fibers would produce a tensile stress, Figure 33b, which will have an effect of lowering the interfacial shear strength. The presence of shrinkage induced compressive stresses is expected to occur in composites having low fiber volume fraction, because in that system each fiber will have a higher likelihood of being surrounded by matrix. Whereas in high fiber volume fraction composites, the fibers would be touching each other and the second mechanism (Figure 33b) is more likely to be present. The calculated fiber volume fractions for the composites tested in this study range from 33 to 45% (see Table 5), which is on the lower side. Therefore, in these composites the first shrinkage mechanism (Figure 33a) is believed to dominate. Thus, we can say that cooling the composite from room to liquid nitrogen temperatures produces an additional ‘clamping force’ on fibers by the matrix, i.e. the composite at the low temperature would have higher interfacial shear strength. The evidence of increase in shear strength can be seen by comparing the photographs of failed samples in

Figure 29 and Figure 30. We can see that the length of the debonded zone (appearing as discoloration in the samples) around the middle of samples at 77K is longer than that at 295K. Experimental data on the effect of interfacial shear strength on flexural elastic modulus and strength of graphite/epoxy composites show that while flexural elastic modulus remains relatively unchanged, the strength increases with an increase in interfacial shear strength [3]. Assuming that glass/epoxy composites have similar sensitivity to interfacial properties, it is expected that the flexural strengths of all three glass/epoxy samples are higher at 77K.

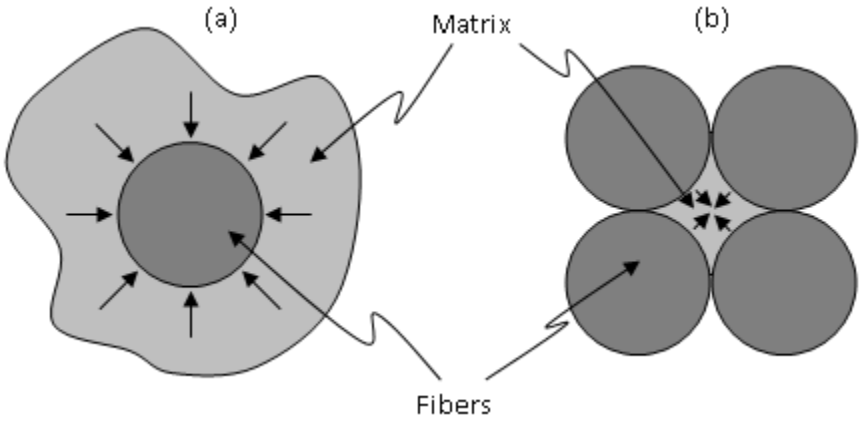

Figure 33. a) Resin shrinkage applying transverse compressive stress on fibers, and b) resin shrinkage applying transverse tensile stress on fibers.

The extended white areas may also indicate increased crazing in the epoxy at low temperature. Crazing is a network of fine cracks that is seen in areas of high hydrostatic stress or areas of exceedingly localized yielding. Unlike a crack, a craze can continue to support load, so the process of craze growth prior to cracking would absorb fracture energy and, in effect, increase the fracture toughness of a polymer [24]. Characteristics

of crazing that are seen in Figure 29 and Figure 30 include a whitening of the crazed region and the fact that crazes tend to propagate perpendicular to the applied tension. Shear bands also have these characteristics; however, crazing occurs in regions that experience an increase in volume while shear banding will be seen under compression [24]. As stated previously, due to the relatively low fiber volume fraction the epoxy will be experiencing tensile stresses indicating crazing rather than shear banding.

Scanning Electron Microscopy (SEM)

Scanning electron microscopy was used to study the failure surface of the 3-point-flexure samples, specifically the bonding between the fibers and the epoxy at the fracture. SEM photomicrographs of the tensile fracture surfaces of the room temperature samples can be seen in Figure 34. Fiber pull-out that occurred before failure is seen in each of the three cases. However, the 1581 and 7781 types show similar characteristics in that there are many small bundles seen as opposed to the one large brush like bundle seen in the 38050 type. It is only natural that the 1581 and 7781 fibers would exhibit similar fiber pullout due to the similarity in their fiberglass cloths. Due to its much larger size, different weave, and lack of fiber surface treatment, the 38050 fibers would be expected to look much different. When comparing the room temperature samples to the samples that were tested under liquid nitrogen, the fiber pull out seen in Figure 35 is significantly less than what was seen in Figure 34. This again is due to the increased clamping forces the matrix places on the fiber, as well as the

increase in fracture toughness caused by the increase in crazing as the temperature is lowered.

(a)

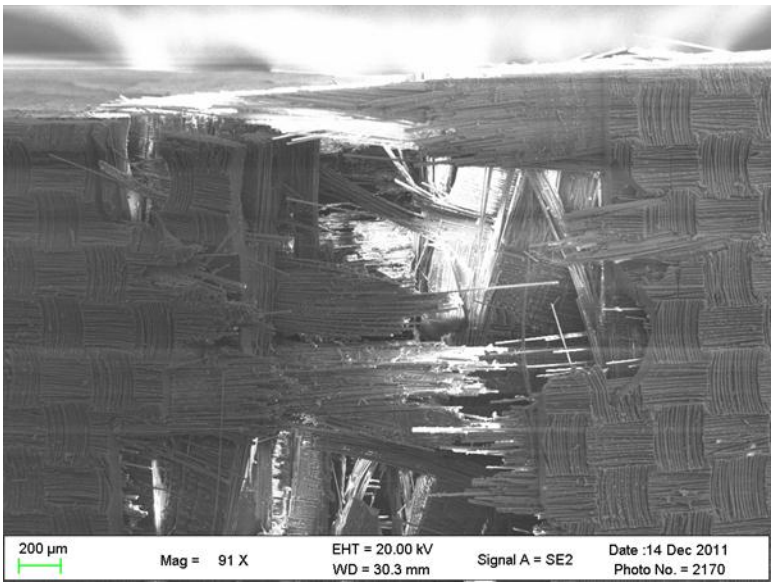

(b)

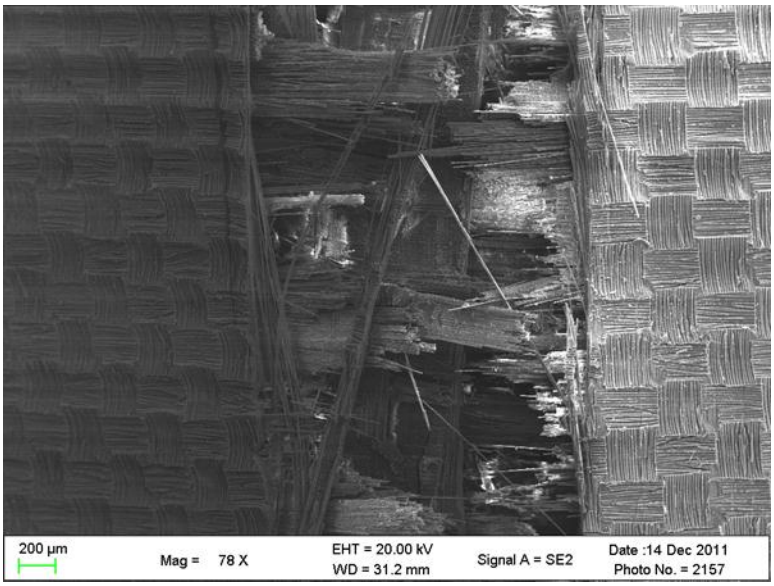

(c)

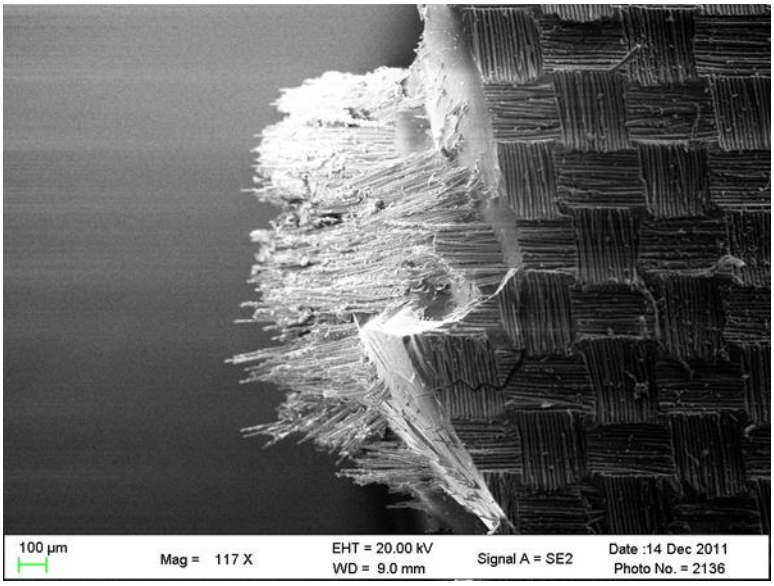

Figure 34. SEM photomicrographs of the tensile region of the room temperature samples for a) 1581/epoxy laminate b) 7781/epoxy laminate and c) 38050/epoxy laminate.

(a)

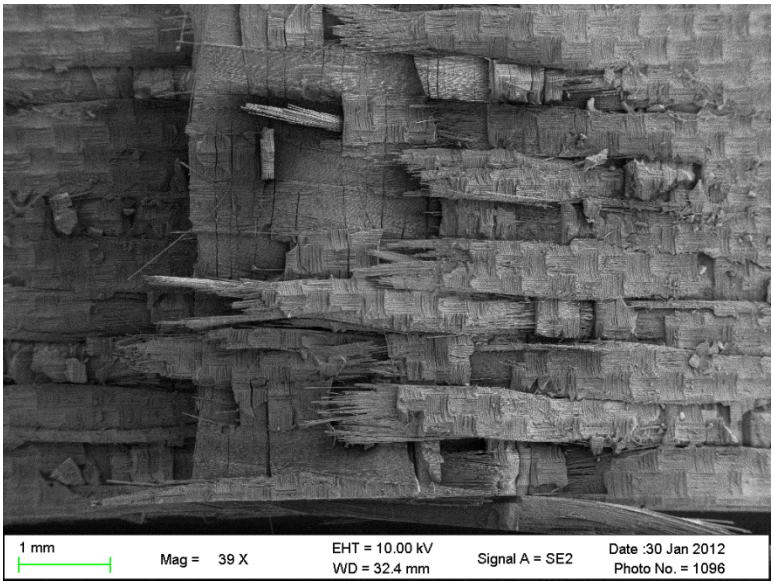

(b)

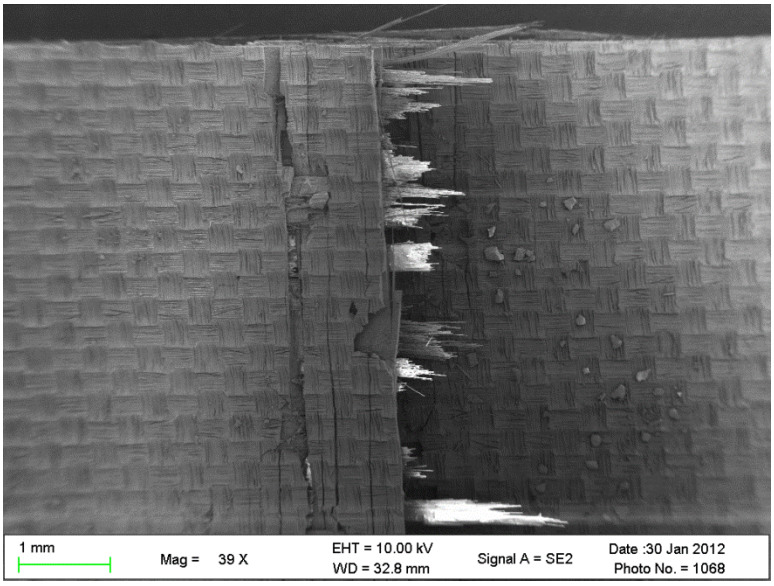

(c)

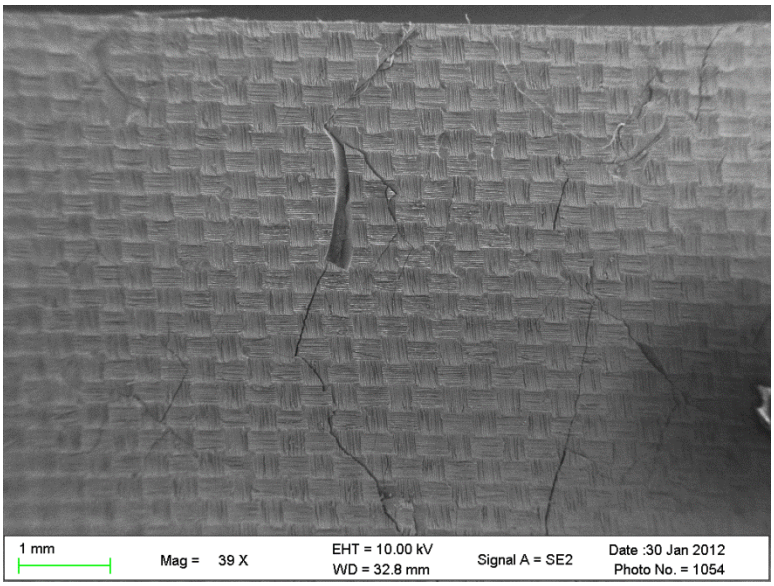

Figure 35. SEM photomicrographs of the tensile region of the liquid nitrogen temperature samples for a) 1581/epoxy laminate b) 7781/epoxy laminate and c) 38050/epoxy laminate.

A closer look at individual fibers can be seen in Figure 36 which allows for evaluation of the bonding between the glass fibers and the epoxy matrix. Based off of these three photomicrographs, it seems necessary to compare the samples in two different groups: first compare the 1581 and 7781 types to the 38050 type and then compare the 1581 to the 7781. As seen in Figure 36c, the glass fibers seem to still be fairly embedded in the epoxy matrix compared to Figure 36a and b. This would cause one to think the compatibility between the 38050 tape and epoxy is greater than the other two. This, however, would not agree with the data reported from the 3-point flexure tests. A likely explanation for this is that the 38050/epoxy laminate failed before a load was reached that would cause significant debonding between the glass fiber and epoxy. With the flatter weaves and lower fiber crimp, the 1581 tape and 7781cloth are able to be much more flexible than the 38050 tape. This would allow for much more ductility, or deformation before failure, in the laminate sample of the former two with the added benefit of more plies for increased strength. The 38050 tape on the other hand has a thick, plain weave that would be much stiffer and allow for minimal deformation of the glass fibers before failure. When this is combined with the large gap between the failure strengths, it seems that the strength of the 38050 laminate relied more on the strength of the epoxy than the strength of the glass fibers which is why there is minimal debonding seen in this sample.

The 1581 fiber/epoxy bonding can now be compared to the 7781 fiber/epoxy bonding. While neither type of fiber is left smooth, there is a difference in the amount of

epoxy seen on each of them. There is some epoxy residue still adhering to the 1581 glass fibers, however Figure 36a reveals an almost absence of the matrix around the ends of the fibers. Figure 36b, on the other hand, shows much more epoxy debris still attached to the fibers. The increase of epoxy around the 7781 fibers indicates a better interfacial bond between fiber and matrix. The amount of matrix around the fibers in both the 1581 and 7781 increases as the temperature was lowered (Figure 37) indicating an increase in the interfacial bond strength between the fiber and matrix as the temperature is lowered as well. The 38050/epoxy laminate fractured at the tensile side during the liquid nitrogen testing, however, when the load was removed, the sample returned to its original position with only cracking left on the tensile surface. Since there was no fiber pull out to study, it was omitted from Figure 37.

(a)

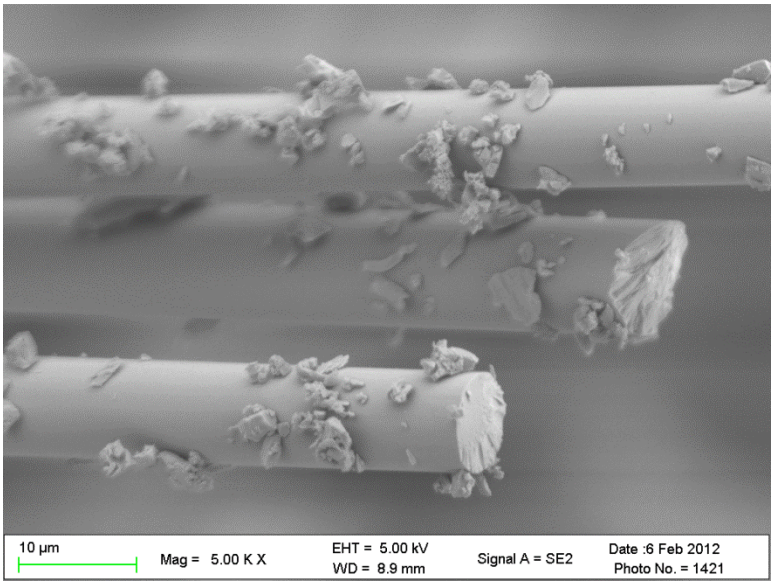
10 µm
Mag = 5.00 K X
EHT = 5.00 kV
WD = 8.9 mm
Signal A = SE2
Date :6 Feb 2012
Photo No. = 1421

(b)

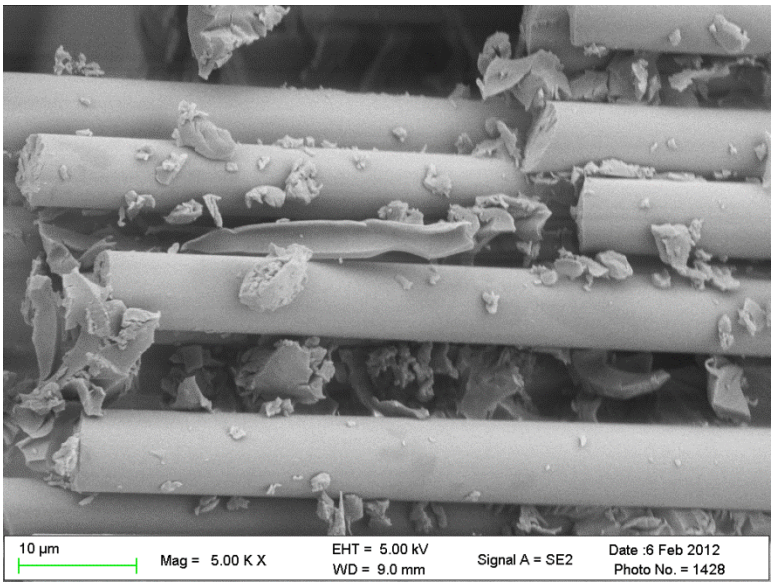
10 µm
Mag = 5.00 K X
EHT = 5.00 kV
WD = 9.0 mm
Signal A = SE2
Date :6 Feb 2012
Photo No. = 1428

(c)

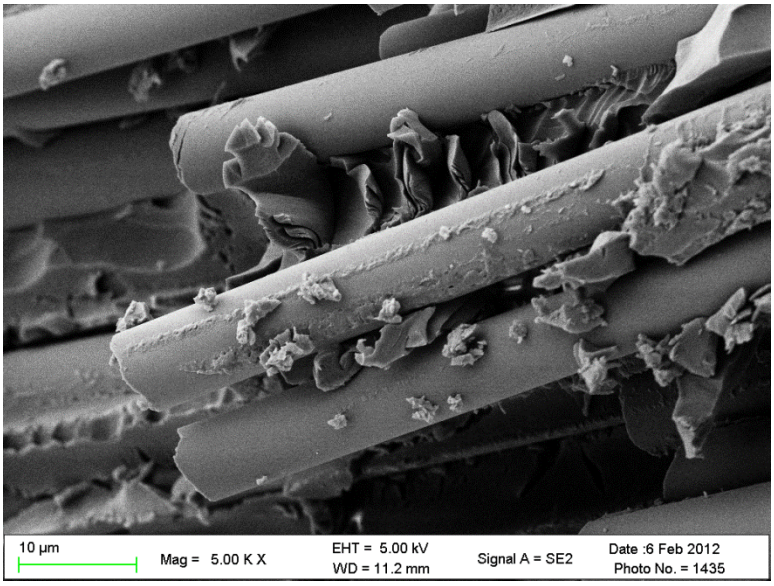

Figure 36. SEM photomicrographs of individual fibers in the tensile region of the room temperature samples for a) 1581/epoxy laminate b) 7781/epoxy laminate and c) 38050/epoxy laminate.

(a)

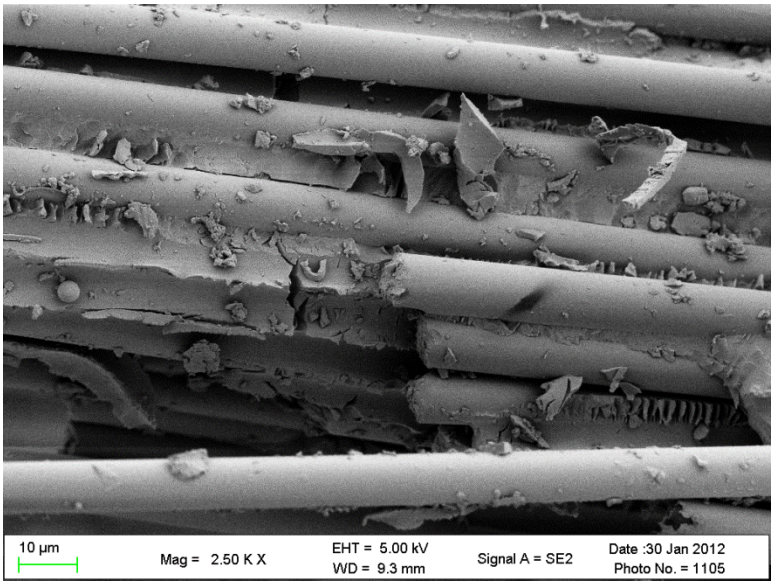

(b)

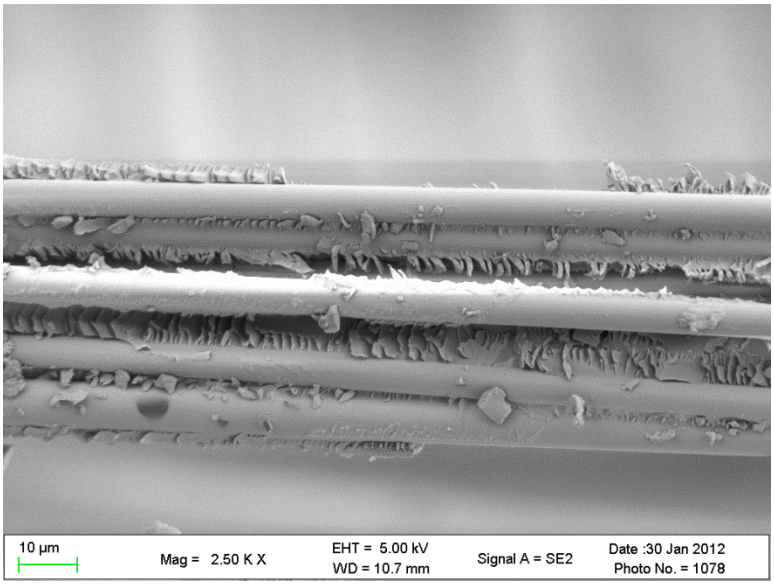

Figure 37. SEM photomicrographs of individual fibers in the tensile region of the liquid nitrogen temperature samples for a) 1581/epoxy laminate and b) 7781/epoxy laminate.

Constant Load Flexural Creep

Representative plots for the three types of laminates at each load showing the displacement as a function of time can be seen in Figure 38.

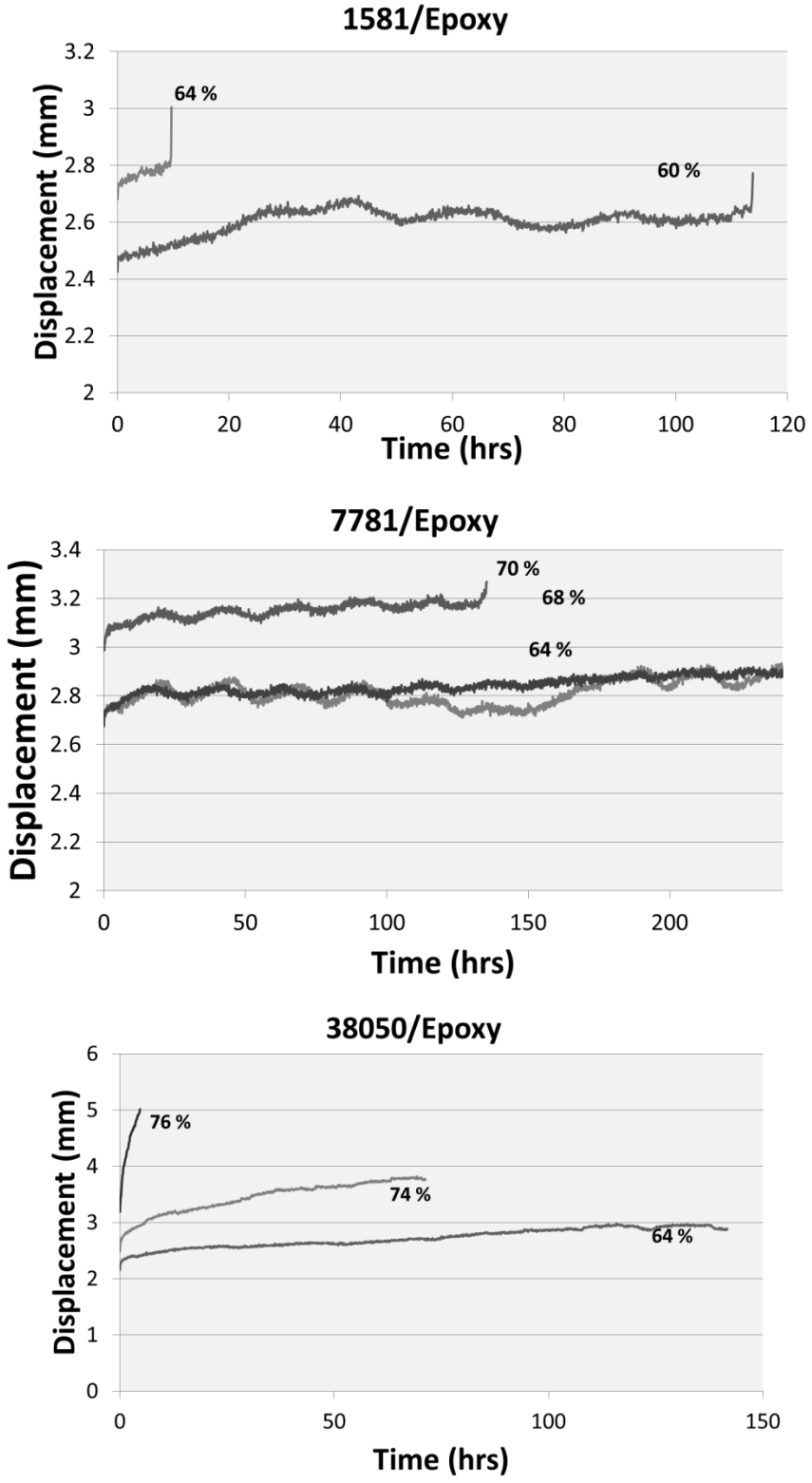

Figure 38. Representative plots of displacement as a function of time for each of the laminates at three different loads. Loads are given in % of Failure Load.

An unusual cyclic pattern is seen in the displacement-time plots in Figure 38, specifically the 7781/epoxy samples. It is also seen in the 1581/epoxy samples, however it seems to be absent in the 38050/epoxy samples. This pattern in the data suggests that the environmental temperature had an impact on the strain the samples experienced. The creep tests were run at room temperature, however, the testing took place in a lab located in a warehouse and the testing apparatus was also located near an outside wall of the lab. It is known that viscoelastic properties change with a change in temperature [15]. The data shows that the change in environmental temperature throughout the day had more of an effect on the test than what would be desired. If you look at the difference in time between each peak and the next valley, the 12 hour difference suggests that the cyclic fluctuations are caused by the change in temperature from night to day. Further evidence that the environmental temperature was the cause for this fluctuation is the time of year each type of laminate was tested. The 38050/epoxy laminate was the first set of samples to be tested. They were tested at the end of summer/beginning of fall in 2011. The difference in temperature between night and day during this time was not a significant amount in the laboratory since the air conditioner was able to keep the inside temperature fairly constant. The data collected for these samples supports this in that the 24 hour cycle seen in the other types of laminates was not seen for this laminate, Figure 38. The most significantly impacted data was the 7781/epoxy laminate samples which had their testing completed during the winter months. The temperature in the laboratory was the most difficult to hold constant during this period. The heat was set to a low enough temperature that the

outside temperature was able to cause significant changes inside during these months. This change in temperature is very apparent in the data recorded. It is likely that the increase in displacement of a sample corresponds to a decrease in the stiffness of the sample caused by an increase in environmental temperature. This increase continues until a peak in the temperature is reached and the temperature again starts to decrease over the next 12 hours until a minimum in the valley is reached corresponding to a lower value in the displacement of the sample likely due to an increase in stiffness. However, further testing is necessary to determine if the cyclic behavior is an indication that the material is responding to the temperature changes. Other possibilities are that the test fixture itself is expanding or contracting or that the LVDT or load cell are being affected with the temperature change. It is recommended to test these possibilities further.

The creep strain was calculated at the specified time using

$$Maximum\ Flexural\ Strain = \frac{6\,\delta_{\max}\,t}{S^2} \qquad \text{…….. (4}$$

and the creep modulus was calculated by dividing the initial stress by the strain at the time specified. These values were then plotted as a function of time to show the time dependent behavior of the laminates. Representative plots of the creep strain at three different stress levels for each laminate type can be seen in Figure 39. The effect of the environmental temperature on the strain was not corrected when plotting the creep modulus. The uncorrected creep modulus of the laminates that correlate to those strains can be seen in Figure 40. The creep modulus was plotted with the time schedule 1, 5, 15, and 30 min; 1, 2, 20, 50, 100, 200 hrs per the ASTM Standard D-2990 [21]. The uncorrected creep modulus curves plotted with data taken every five minutes can be

seen in Appendix II. The uncorrected creep modulus for the laminates at the different loads was approximated from the curves with more data points.

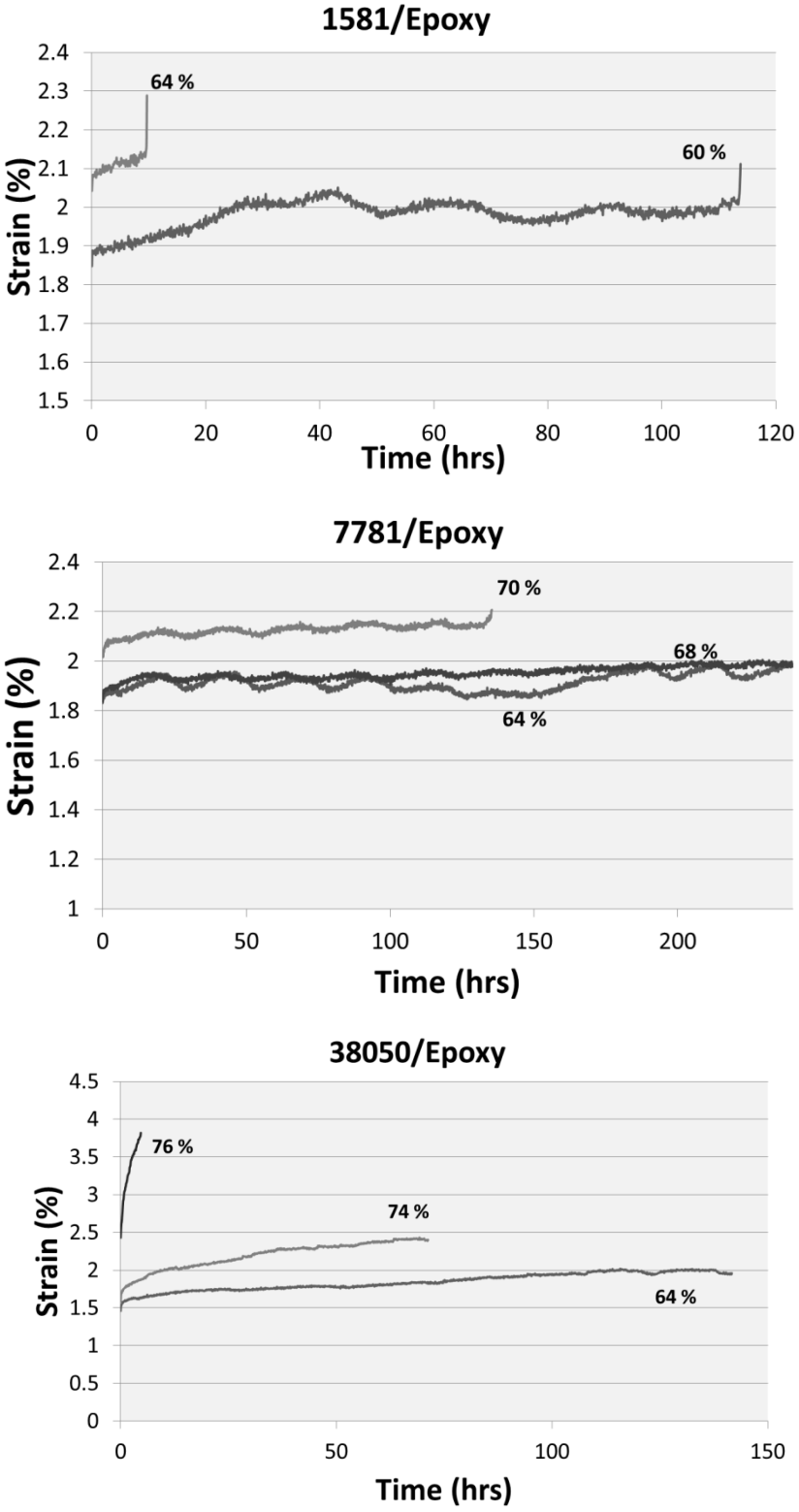

Figure 39. Representative plots of strain as a function of time for each of the laminates at three different loads. Loads are given in % of Failure Load.

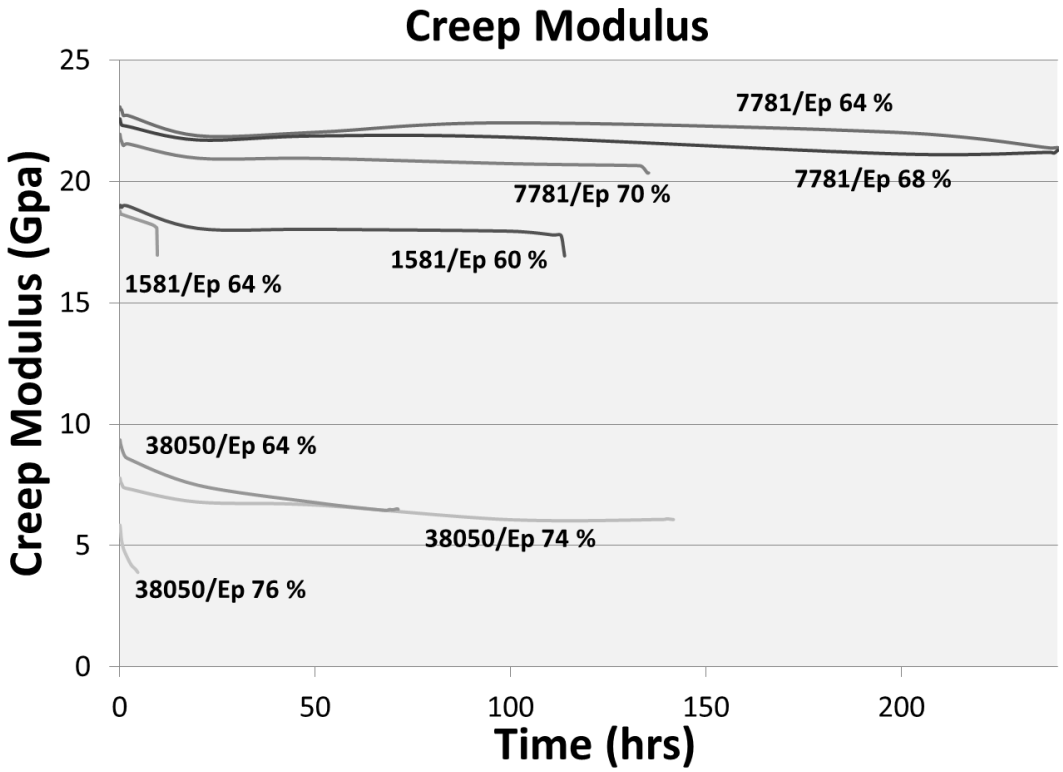

Figure 40. Representative uncorrected creep modulus curves for all laminates at each load tested.

The key observations from these charts are as follows:

(i) While the data seems to be noisy due to the cyclic behavior, the overall trend of the creep is consistent.

(ii) The 7781/epoxy laminate experienced a smaller amount of strain at higher loads, performing the best out of the three laminate types. The 38050/epoxy laminate performed the poorest experiencing the highest strains at the lowest loads. The poor performance of 38050/epoxy can be attributed to the low

areal density of both 38050 glass tape and the density of 38050/epoxy composites.

(iii) The 7781/epoxy laminate was able to sustain creep at higher percentages of its failure load without rupture than the 1581/epoxy laminate. While the short-term testing showed that the 7781/epoxy laminate had a higher strength than the 1581/epoxy laminate, this could partially be due to the samples not having been kept in a moisture free environment. Since the 1581/epoxy laminates were the last to be tested, it is possible that moisture absorption occurred over time in the samples affecting the strength of the material. Further testing is needed.

(iv) The strain experienced by each laminate decreases with decreasing load.

(v) Tertiary creep is seen in all samples that ruptured (1581/epoxy: 60 and 64%; 7781/epoxy: 70%; 38050/epoxy: 76%). Testing ended during the secondary creep stage for the remaining samples.

(vi) The lack of linearity in the steady- state stage (secondary) is most likely due to the change in environmental change. Typically, an increase in temperature at a constant stress will decrease the amount of time required to provide an equal strain at a lower temperature [25]-[27].So a change in temperature will affect the linearity of the strain curve.

(vii) The approximate creep moduli for the laminates at the different loads are summarized in Table 4. The creep modulus for each type of laminate decreases with increasing load. The only exception to this is the 38050/epoxy

laminate at 64 and 74%. However, the creep test for the sample at 64% was cut short due to a power outage. Comparing the trends of the two moduli, the one at 74% of the failure load is leveling off while the one at 64% of the failure load is still steadily decreasing. It is possible that if the data from the whole test had been recorded that the moduli would have lined up like the rest.

Table 4. Approximate Uncorrected Creep Moduli for Laminates at Tested Percentages of Failure Loads

Type of Laminate	Creep Modulus at Load 1 (Gpa)	% of Short-Term Modulus	Creep Modulus at Load 2 (Gpa)	% of Short-Term Modulus	Creep Modulus at Load 3 (Gpa)	% of Short-Term Modulus
1581/Epoxy			17.2@ 60%	86	16.9 @ 64%	84.5
7781/Epoxy	21.3 @64%	96.2	21.1 @68%	95.3	20.4 @70%	92.1
38050/Epoxy	5.9 @ 64%	77.9	6.5 @74%	85.9	4.1 @76%	54.2

(viii) Table 4 also shows the correlation between the creep modulus and the short-term modulus found in the flexure tests. Overall, as the percentage of failure load on the sample decreases, the percentage of the short-term modulus that is seen in the creep modulus increases.

CHAPTER V
CONCLUSIONS AND RECOMMENDATIONS

Conclusions

Compatibility of three different glass cloth/tape products (1581, 7781, and 38050) with an epoxy matrix was evaluated using 3-point bend tests by loading them to failure at 295K and 77K using 3-point bend tests. These glass products varied in the type of weave patterns (plain versus 8-harness satin weave), aerial density of the cloth, and fiber surface treatment (epoxy compatible surface treated versus untreated). The experimental data lead to the following conclusions:

a) 1581/epoxy and 7781/epoxy, both having 8-harness satin weave and both having epoxy compatible surface treatment, and higher laminate densities had much higher flexural elastic modulus and strength compared to those of 38050/epoxy which contained untreated glass fibers in a plain weave.

b) The correlation of composite density with the laminate's flexural elastic modulus and strength showed an almost linear relationship. Since all laminates were fabricated under equivalent conditions, this indicates that the flexural properties were dependent on the relative glass content of the glass cloth and not by the lack of an epoxy-compatible finish on the glass fibers.

c) Failure pattern examination showed the evidence of an increase in interfacial strength when temperature is lowered from 295K to 77K.

d) While the flexural elastic modulus of all three composites increased only modestly (by about 5-10%) at the low temperature, the strength registered an increase of almost 50%.

e) From comparison of both the temperature dependence of each flexural property and the density dependence of each property, one can conclude that (1) the flexural modulus is dominantly dependent on the glass content and (2) the flexural strength is dependent on both glass content and the resin strength.

f) The preliminary constant load creep data showed that the 7781/epoxy laminate had the best time-dependent behavior of the three laminate types.

Recommendations

Following this study on the comparison of the 7781/epoxy, 1581/epoxy, and 38050/epoxy laminates, it is recommended that further evaluation of the long-term behavior of the material be studied. While this study gave a preliminary look at the creep behavior of the laminates, there is still much to be studied about the long term-behavior. A more in depth study that would provide the time needed to run creep rupture tests at multiple loads would allow a rupture envelope to be created for each of the laminates. Also, allowing the time to let the laminates sit under a load for a longer period (1000hrs) will provide much more information on the behavior of the laminates and would allow for modeling of the creep data to provide a way to predict the time to rupture at any stress level.

Further recommendation includes a look at how the temperature affected the creep data. While the effect of the temperature on the material is most likely the dominant cause for the cyclic fluctuation in the data, other factors could contribute to this as well. The temperature could have affected the material of the test apparatus, the LVDT or the load cell as well. If a test is run without a sample, these other factors can be tested. By concentrating the temperature change on each of these areas at different times, the data can be evaluated to see the if there is a significant change in what data is recorded and, in effect, determine whether they had a significant effect on the data seen in this study.

Since during the operation of the CS superconducting electromagnets these glass composites will be subjected to liquid helium temperature, it is also recommended that the composites should also be characterized at 4K. Due to the difficulty in handling liquid helium as well as the expense, another way to try and predict the mechanical properties found in this study at 4K would be to characterize the composites at a temperature between 295K and 77K. This would show the curve of the line of a certain property, strength for example, when plotted against temperature and the correlation would be able to be seen as the temperature is decreased allowing for a possible prediction at 4K.

LIST OF REFERENCES

[1] Scultz, J.L, Antaya, T., Feng, J., Gung, C.Y. Martovetsky, N., Minervini, J.V., Michael, P., Radovinsky, A. and Titus, P. (2005). The ITER Central Solenoid, *21st IEE/NPS Symposium on Fusion Engineering*, Knoxville, TN, September.

[2] <www.iter.org>

[3] Gao, X. Jensen, R.E. Li, W., Deizel, J., McKnight, S.H. and Gillespie, J.W. Jr. (2008). Effect of Fiber Surface Texture Created from Silane Blends on the Strength and Energy Absorption of the Glass Fiber/Epoxy Interphase, *J. of Composite Materials*, Vol. 42, pp. 513-534.

[4] Keusch, S. and Haessler, R. (2008) Influence of Surface Treatment of Glass Fibers on Dynamic Mechanical Properties of Epoxy Resin Composites, *Composites*, Part A, Vol. 30, pp. 997-1002.

[5] Thomason, J.L. and Schoolenberg, G.E. (1993). An Investigation of Glass Fiber /Polypropylene Interface Strength and its Effect of Composite Properties, *Composites*, Vol. 25, No. 3, pp. 197-203.

[6] Madhukar, M. S. and Drzal, L. T. (1991). Fiber-Matrix Adhesion and its Effect of Composite Mechanical Properties: II. Longitudinal (0^o) and Transverse (90^o) Tensile and Flexure Behavior of Graphite/Epoxy Composites, *J. Composite Materials*, Vol. 25, pp. 958-991.

[7] Mittal, R. K. (2004). Influence of fiber length, fiber orientation, and interfacial adhesion on poly (butylene terephthalate)/polyethylene alloys reinforced with short glass fibers, *Polymer Composites*, Vol. 26, Issue 1, pp. 1-11.

[8] Singh, B., Gupta, M. and Verma, A. (1996). Influence of fiber surface treatment on the properties of sisal-polyester composites, *Polymer Composites*, 17 (6), pp. 910-918.

[9] Nayak, S. K., Mohanty, S. and Samal, S. K. (2010). Influence of interfacial adhesion on the structural and mechanical behavior of PP-banana/glass hybrid composites, *Polymer Composites*, 31(7), pp. 1247-1257.

[10] Blakley, K. L., Grady, B. P. and O'Rear, E. A. (2004). Effects of styrene-isoprene copolymer glass fiber coatings on woven glass cloth epoxy composite performance, *Polymer Composites*, 25(1), pp. 82-93.

[11] Cecen, V., Sarikanat, M., Yildiz, H. and Tavman, I.H. (2008). Comparison of Mechanical Properties of Epoxy Composites Reinforced with Stitched Glass and Carbon Fabrics: Characterization of Mechanical Anisotropy in Composites and Investigation on the Interaction between Fiber and Epoxy Matrix, *Polymer Composites*, pp. 840-853.

[12] Suppakul, P. and Bandyopadhyay, S. (2002). The Effect of Weave Pattern on the Mode-I Interlaminar Fracture Energy of E-glass/vinyl Ester Composites, *Composites Science and Technology*, Vol. 62, pp. 709-717.

[13] Carolina Narrow Fabrics: Customer Service. (336) 631-3000. Winston Salem, NC.

[14] Reed, R.P., Darr, J.B. and Schutz, J.B. (1992). Shot-Beam Shear Testing of Candidate Magnet Insulators, *Cryogenics*, Vol.32, ICMC Supplement, pp. 9-13.

[15] Callister, W.D. (2007). Material Science and Engineering: An Introduction. John Wiley and Sons. Pp 238-241, 524-531.

[16] Dowling, N.E. (2007). Mechanical behavior of materials, 3rd edition, Pearson Prentice Hall, Upper Saddle River, NJ, p912.

[17] Findley, W.N. (1960). Mechanism and mechanics of creep of plastics, Society of plastics engineers (SPE) journal, 16(1), 57-65.

[18] Roylance, D. (2001), Modulus in mechanics of materials, Massachusetts institute of technology, Cambridge, MA. (http://web.mit.edu/course/3/3.11/www/module_list.html)

[19] Chevali, V.S. and Janowski, G.M. (2010). Flexural creep of long fiber-reinforced thermoplastic composites: Effect of processing-dependent fiber variables on creep response, *Composites: Part A,* Vol. 41, pp 1253-1262.

[20] Yeo, S.S., Evaluation of Creep Behavior of Geosynthetics Using Accelerated and Conventional Methods, Drexel Library Online Archives.

[21] ASTM Standard D 2990 and D790. In: *Annual Book of ASTM Standards, vols. 8.02 and 8.01*. West Choshocken, PA, USA.

[22] Reed, R.P., Evans, D. and Fabian, P.E. (2000). Development of a New Resin System for the U.S. ITER Central Solenoid Modal Coil, *Advances in Cryogenic Engineering-Materials*, Vol. 46A, pp.227-234.

[23] Reed, R.P. and McColskey, J.D. (1994). Composite Struts for SMES Plants, *NISTIR* 5024, National Institute of Standards and Technology, Boulder, Colorado, October.

[24] <http://en.wikipedia.org/wiki/Crazing>

[25] Drozdov, A.D. (2010). Effect of temperature on the viscoelastic and viscoplasticbehavior of polypropylene, *Springer Science+Business Media*, Published online.

[26] Dasappa, P., Lee-Sullivan, P., and Xiao, X. (2009). Temperature effects on creep behavior of continuous fiber GMT composites. *Composites: Part A,* Vol. 40*,* pp. 1071-1081.

[27] Drozdov, A.D., Agarwal, S., and Gupta, R.K. (2004). The effect of temperature on the viscoelastic behavior of linear low-density polyethylene. *Archive of Applied Mechanics,* Vol. 73, pp. 591-614.

APPENDIX I: LOAD DISPLACEMENT DATA

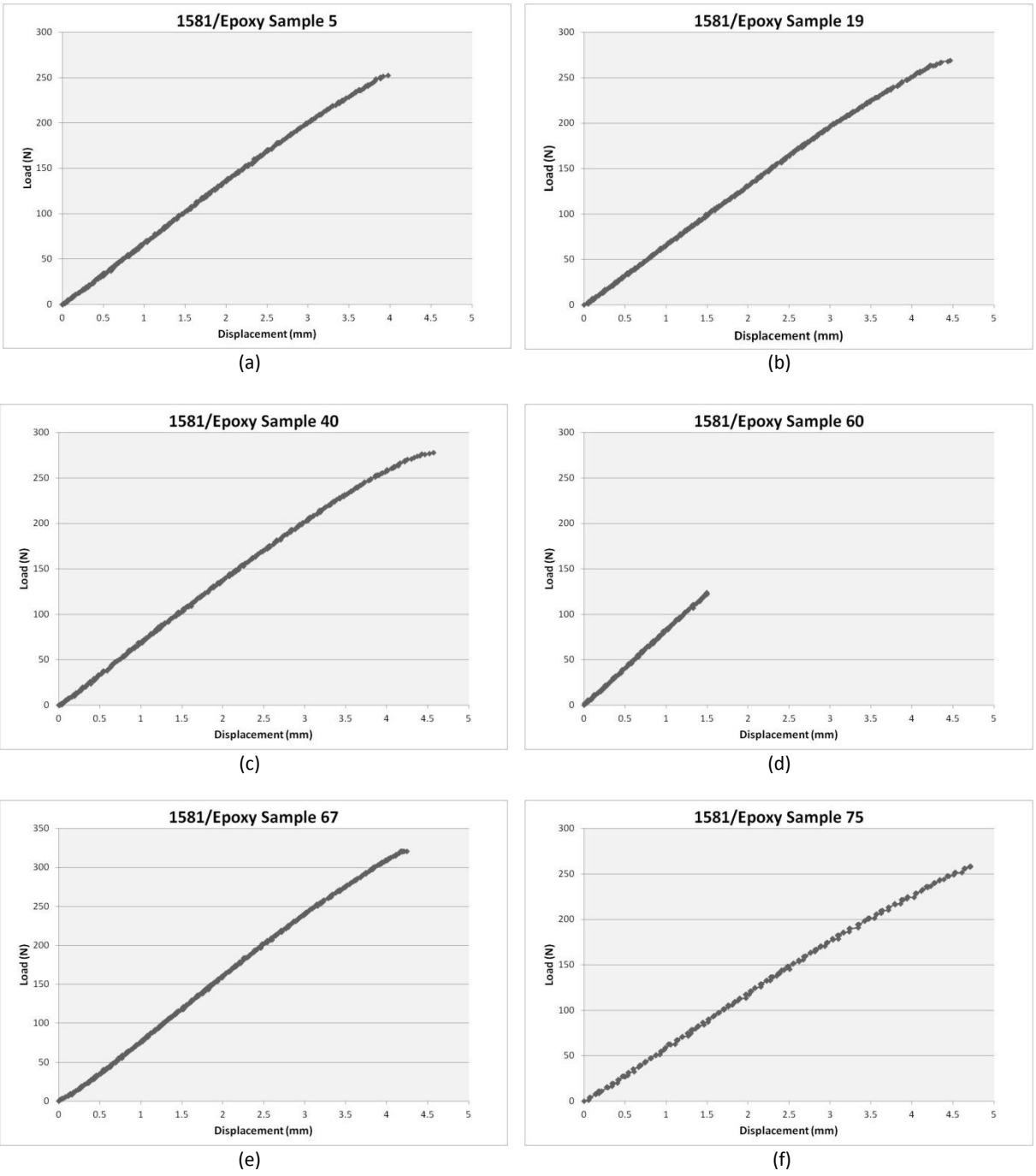

Figure AI. 1. Individual load-displacement results at room temperature for 1581/Epoxy samples.

APPENDIX I: LOAD DISPLACEMENT DATA

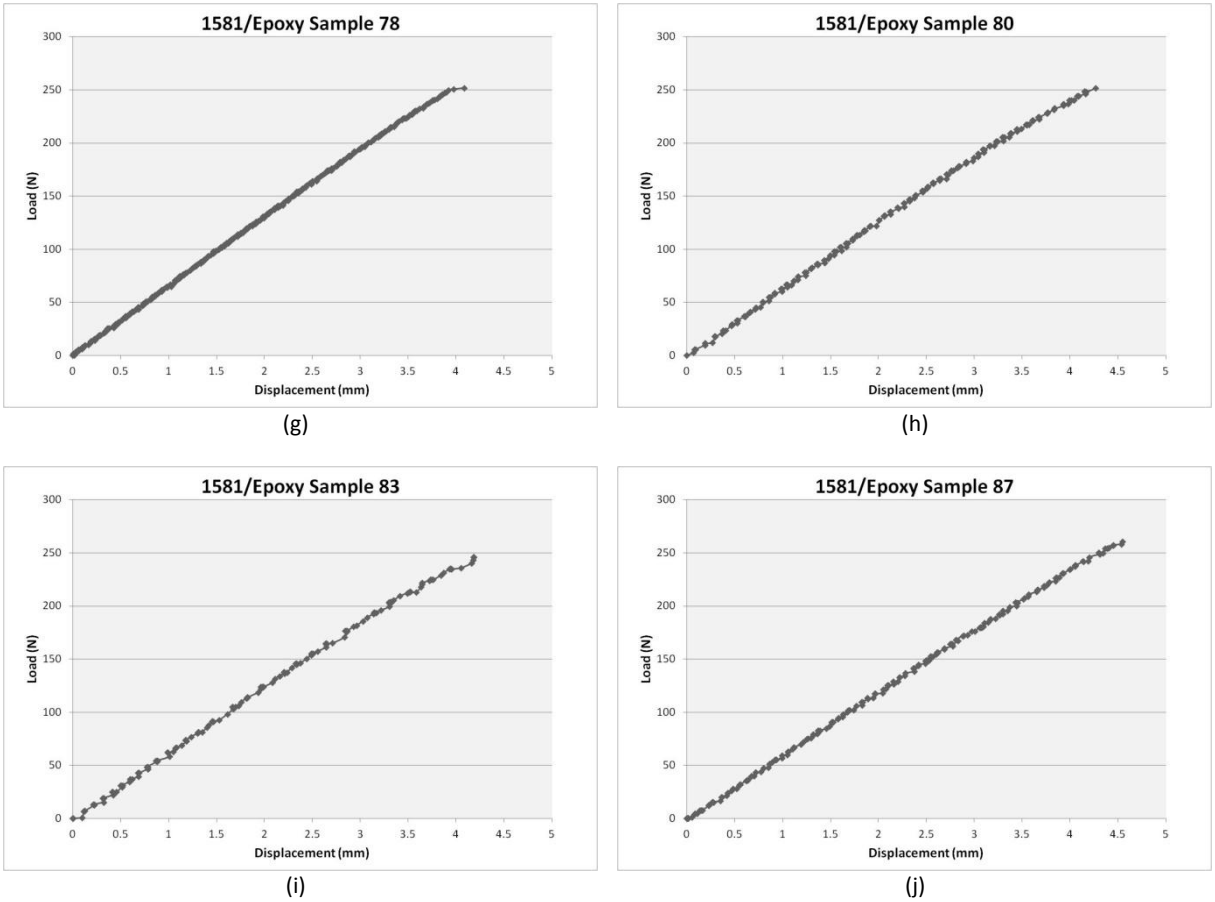

Figure AI. 1 cont. Individual load-displacement results at room temperature for 1581/Epoxy samples.

APPENDIX I: LOAD DISPLACEMENT DATA

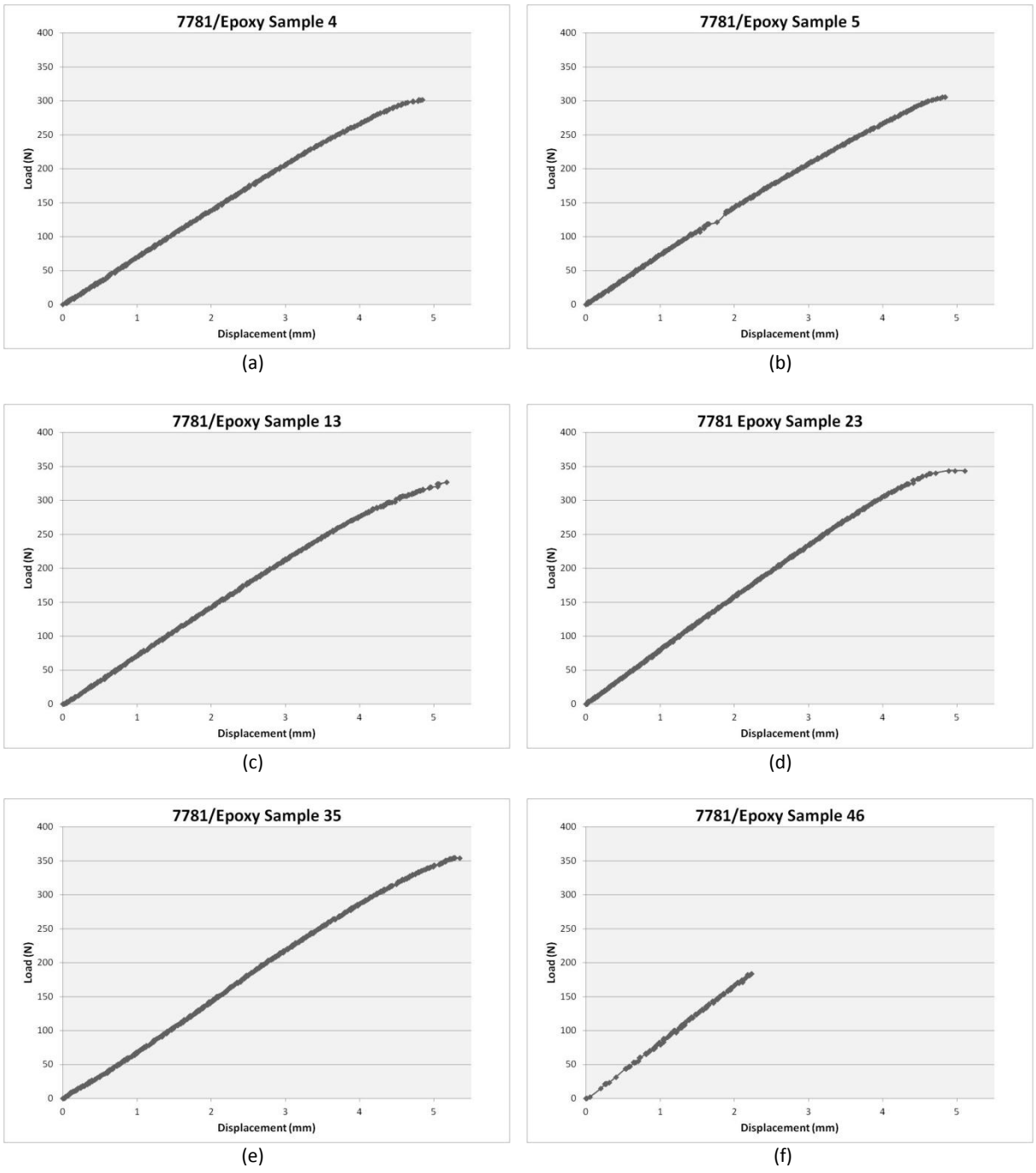

Figure AI. 2. Individual load-displacement results at room temperature for 7781/Epoxy samples.

APPENDIX I: LOAD DISPLACEMENT DATA

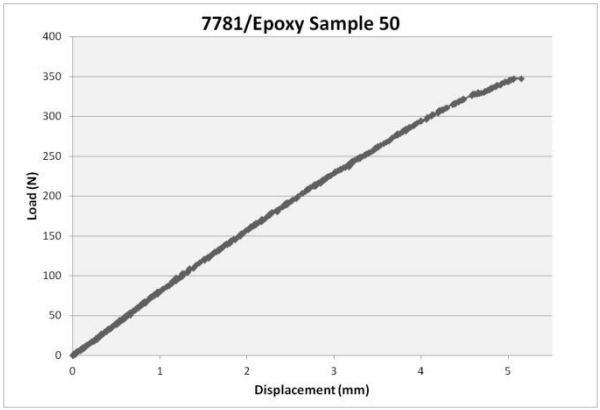

(g)

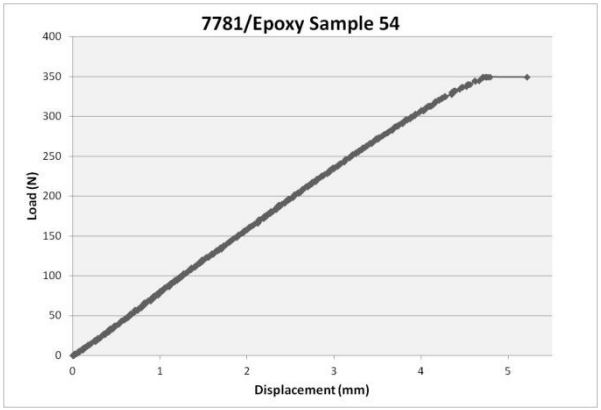

(h)

Figure AI. 2 cont. Individual load-displacement results at room temperature for 7781/Epoxy samples.

APPENDIX I: LOAD DISPLACEMENT DATA

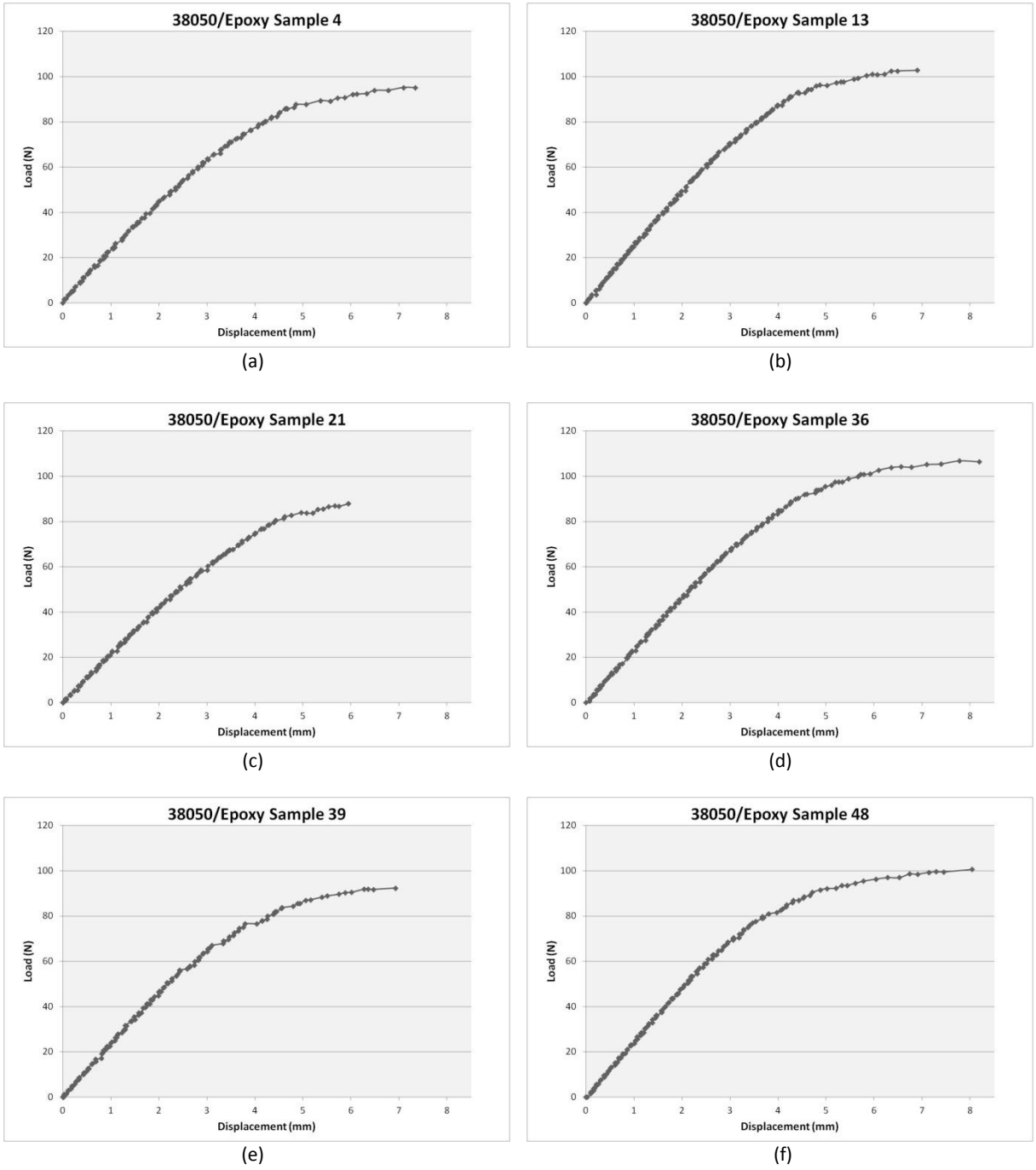

Figure AI. 3. Individual load-displacement results at room temperature for 38050/Epoxy samples.

APPENDIX I: LOAD DISPLACEMENT DATA

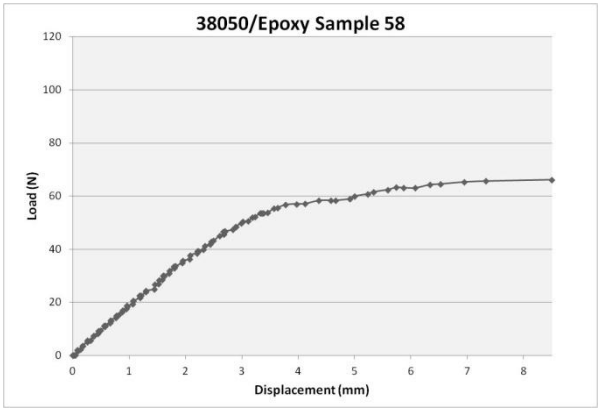

(g)

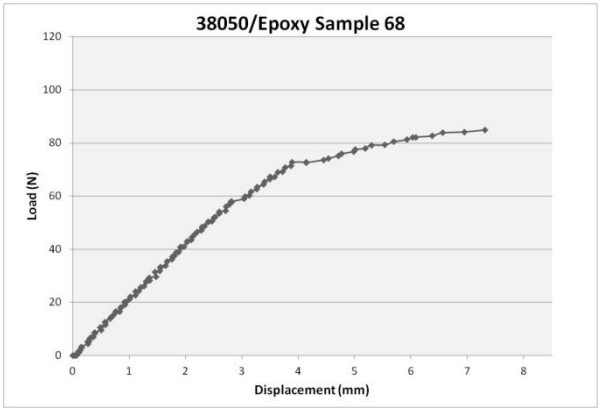

(h)

Figure AI. 3 cont. Individual load-displacement results at room temperature for 38050/Epoxy samples.

APPENDIX I: LOAD DISPLACEMENT DATA

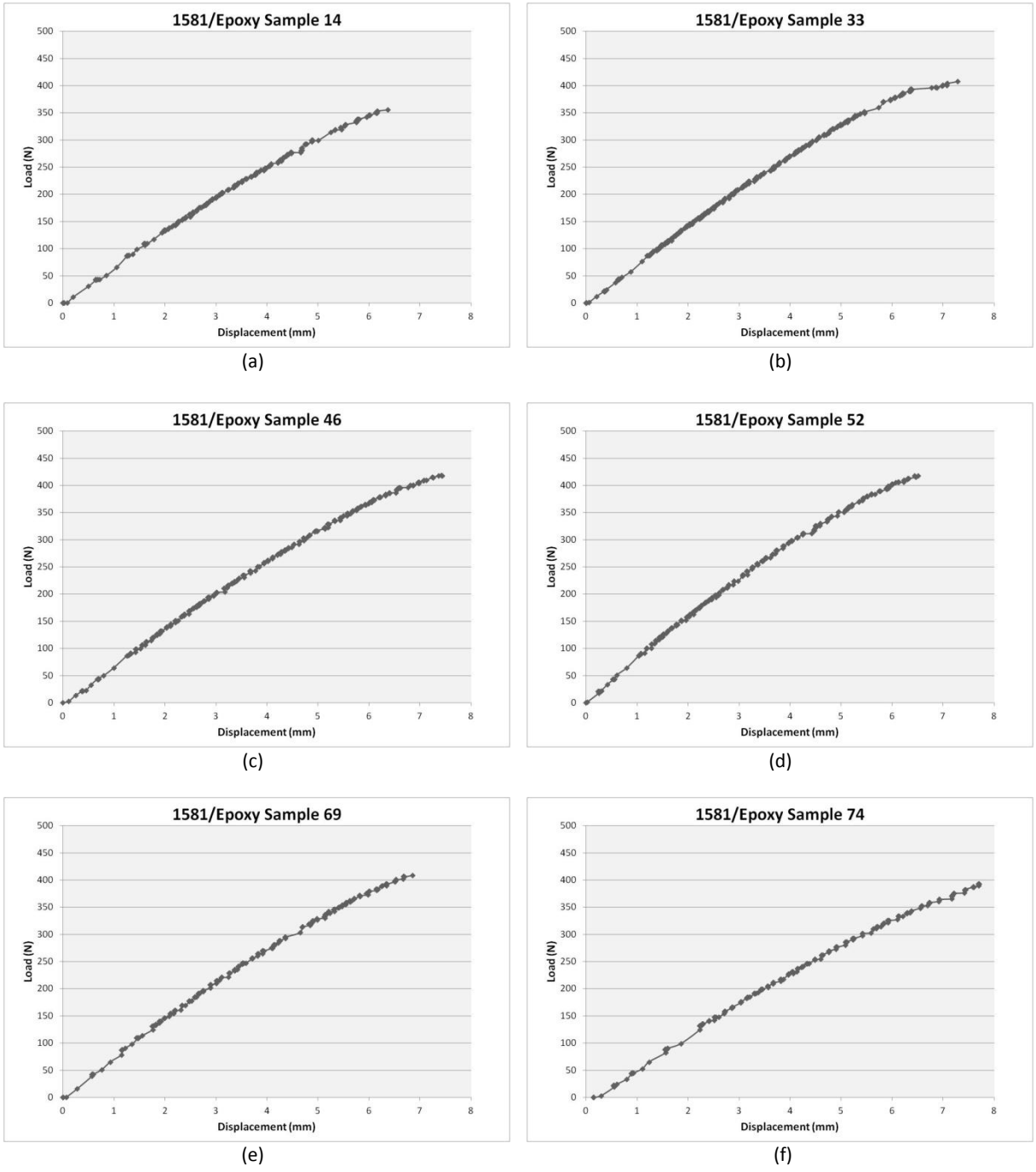

Figure AI. 4. Individual load-displacement results at liquid nitrogen temperature for 1581/Epoxy samples.

APPENDIX I: LOAD DISPLACEMENT DATA

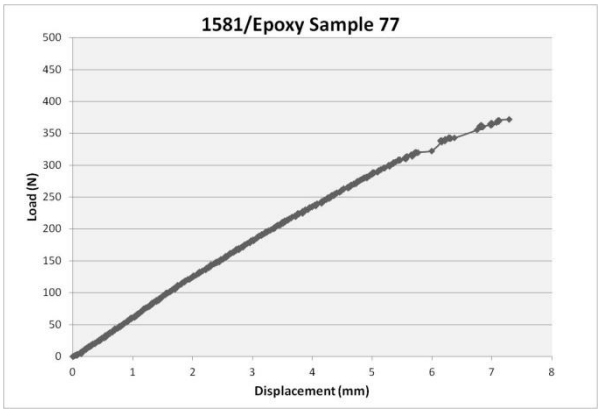

(g)

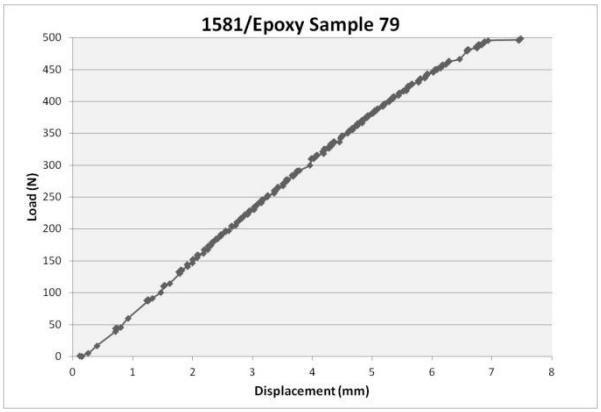

(h)

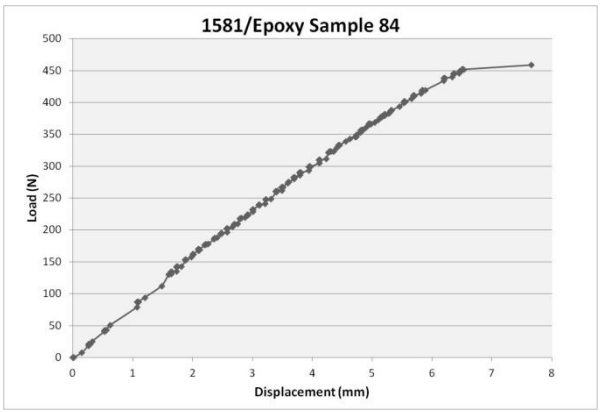

(i)

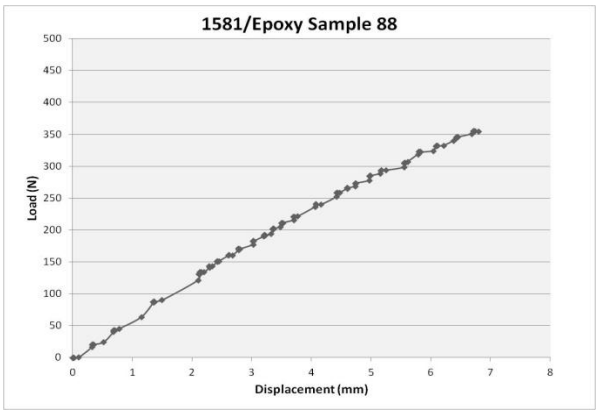

(j)

Figure AI. 4 cont. Individual load-displacement results at liquid nitrogen temperature for 1581/Epoxy samples.

APPENDIX I: LOAD DISPLACEMENT DATA

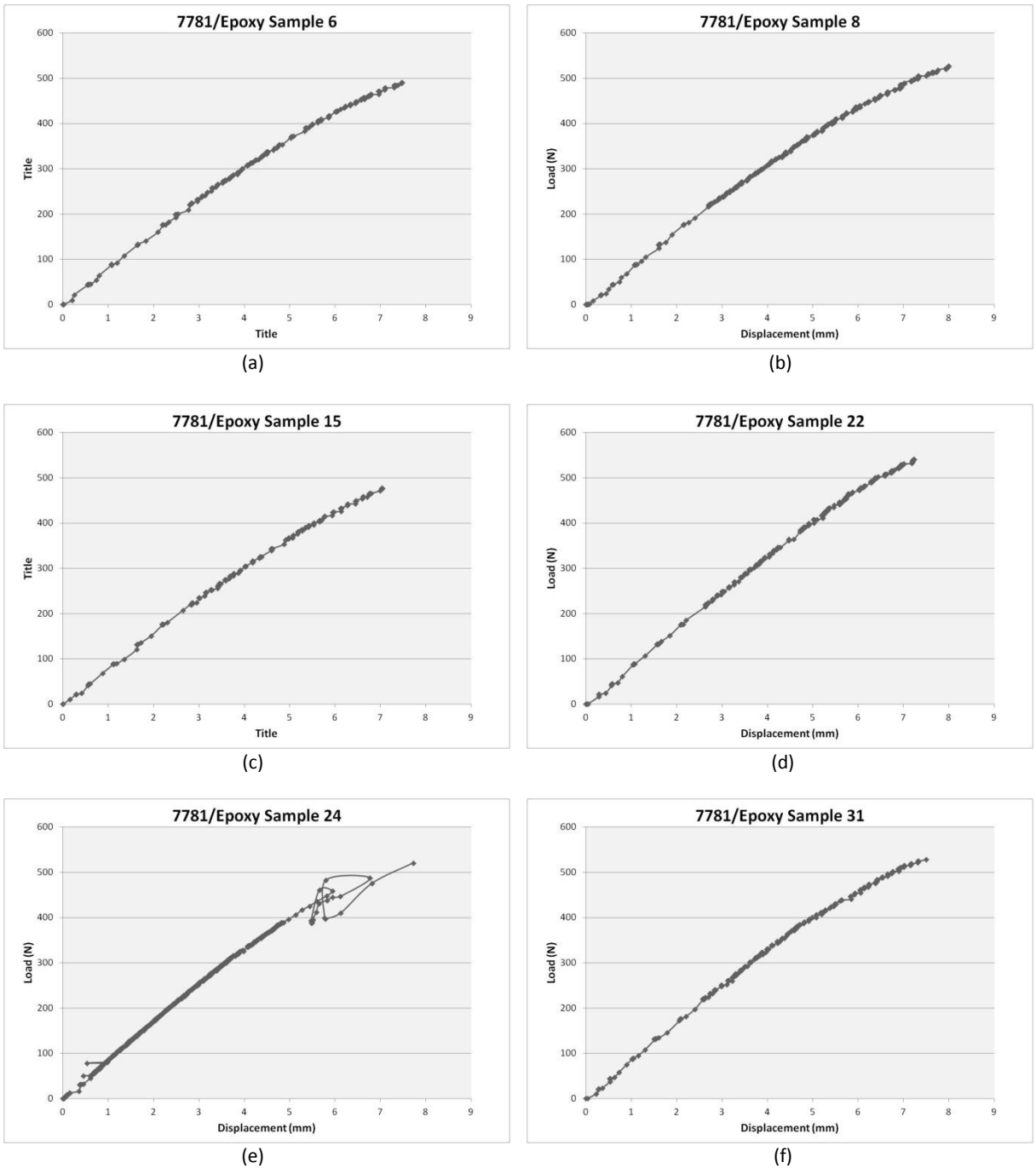

Figure AI. 5. Individual load-displacement results at liquid nitrogen temperature for 7781/Epoxy samples.

APPENDIX I: LOAD DISPLACEMENT DATA

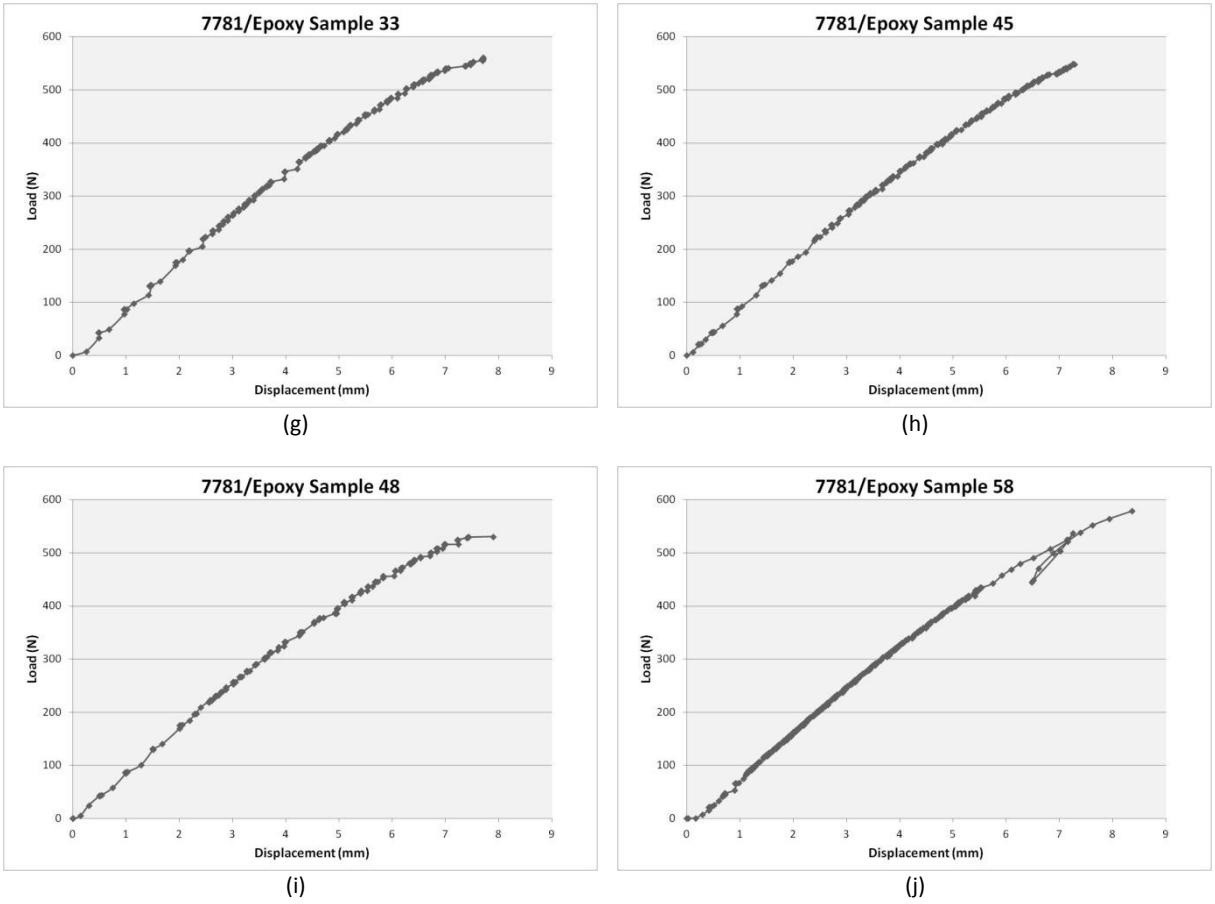

Figure AI. 5 cont. Individual load-displacement results at liquid nitrogen temperature for 7781/Epoxy samples.

APPENDIX I: LOAD DISPLACEMENT DATA

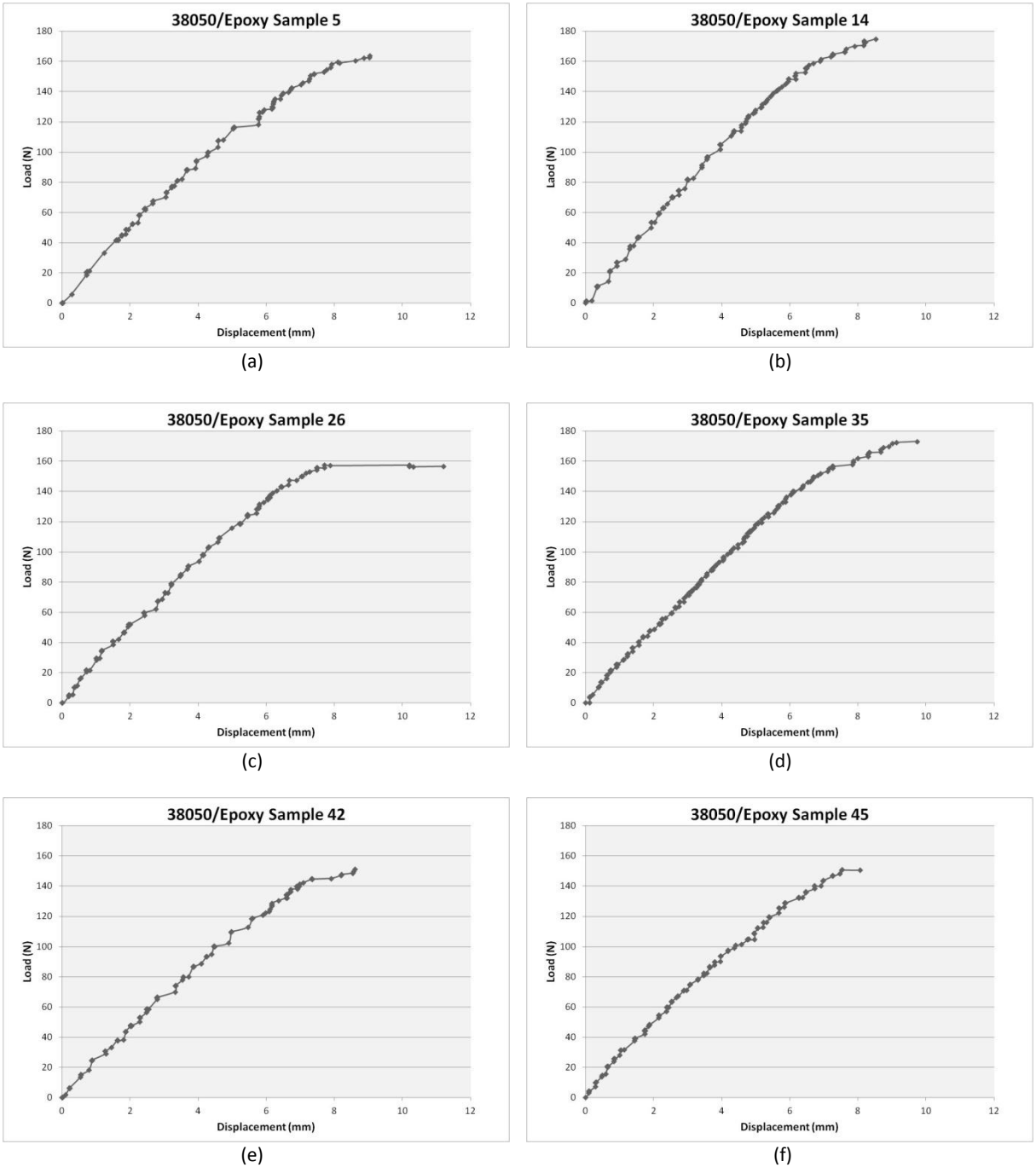

Figure AI. 6. Individual load-displacement results at liquid nitrogen temperature for 38050/Epoxy samples.

APPENDIX I: LOAD DISPLACEMENT DATA

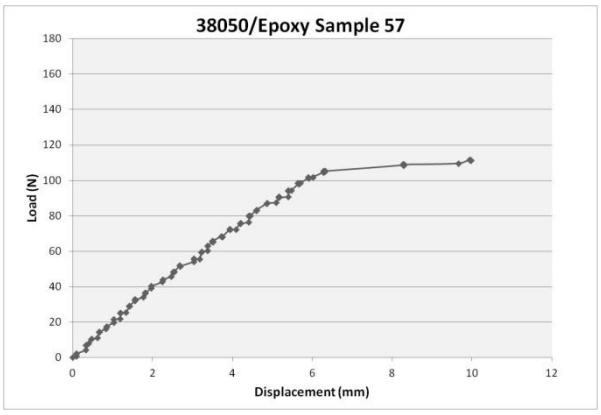

(g)

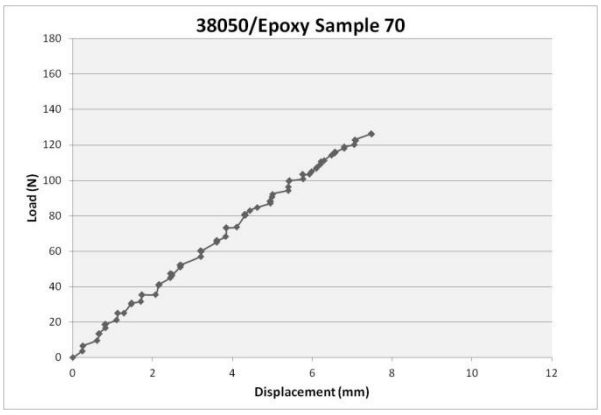

(h)

Figure AI. 6 cont. Individual load-displacement results at liquid nitrogen temperature for 38050/Epoxy samples.

APPENDIX II: CREEP DATA

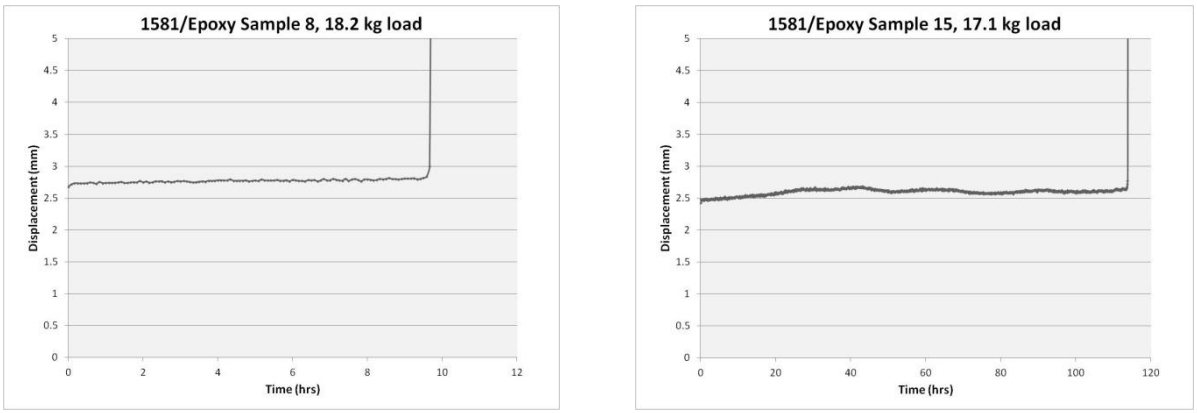

(a) (b)

Figure AII. 1. Individual constant load creep results at room temperature for 1581/Epoxy samples.

APPENDIX II: CREEP DATA

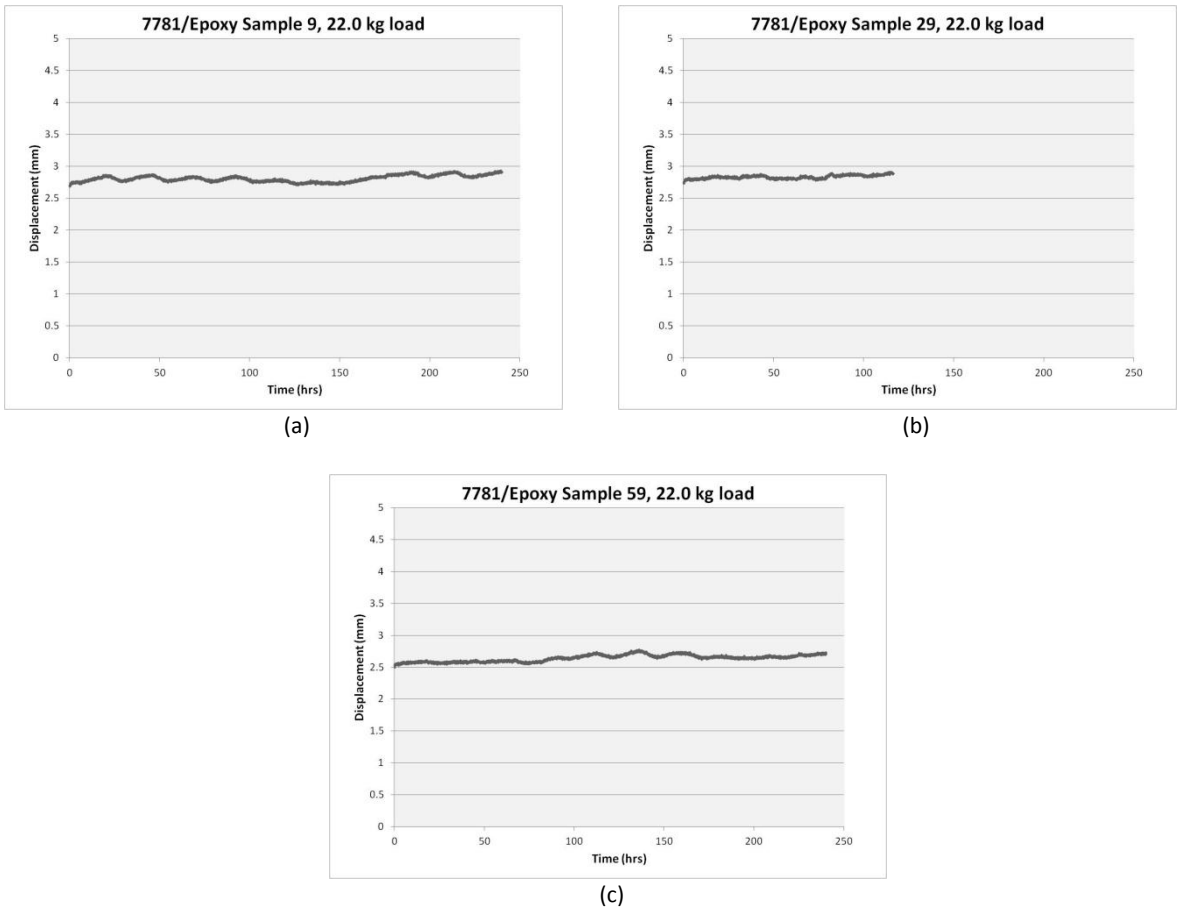

Figure AII. 2. Individual constant load creep results at room temperature for 7781/Epoxy samples.

APPENDIX II: CREEP DATA

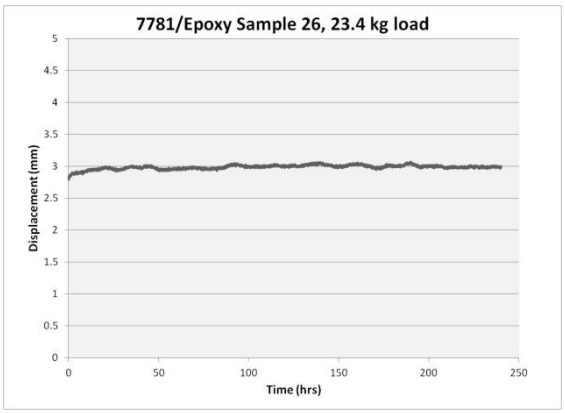

(d)

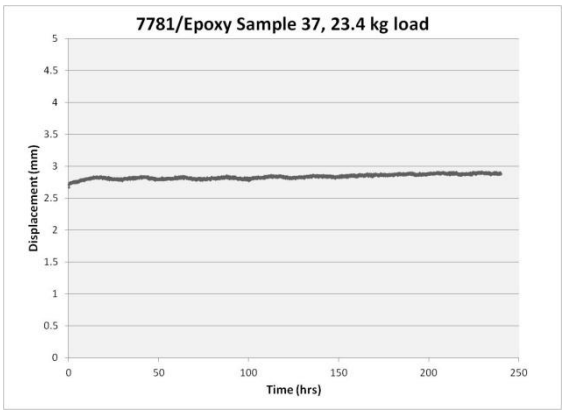

(e)

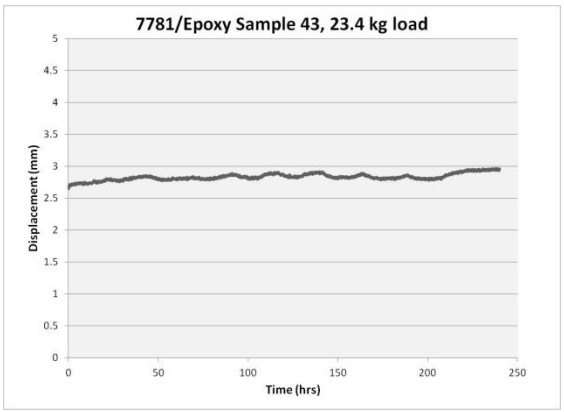

(f)

Figure AII. 2 cont. Individual constant load creep results at room temperature for 7781/Epoxy samples.

APPENDIX II: CREEP DATA

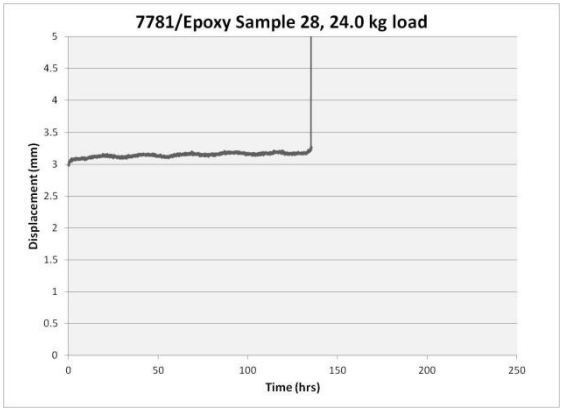

(g)

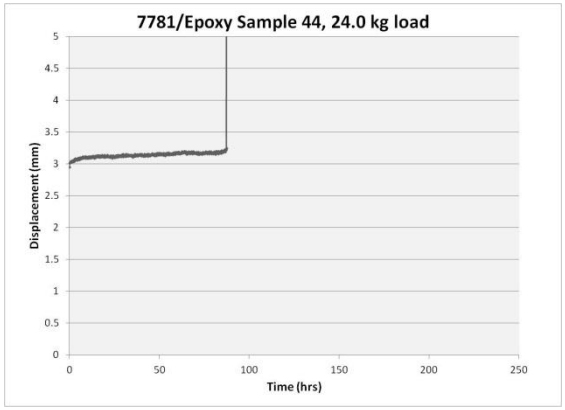

(h)

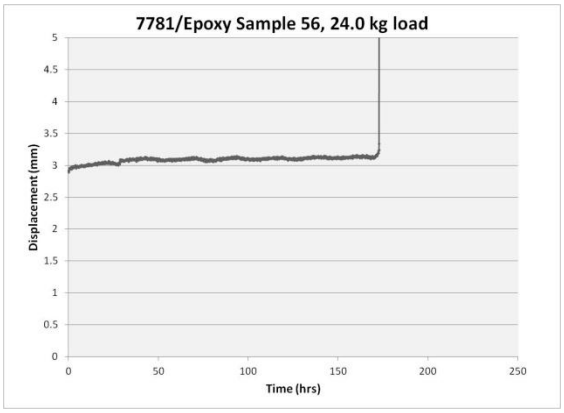

(i)

Figure AII. 2 cont. Individual constant load creep results at room temperature for 7781/Epoxy samples.

APPENDIX II: CREEP DATA

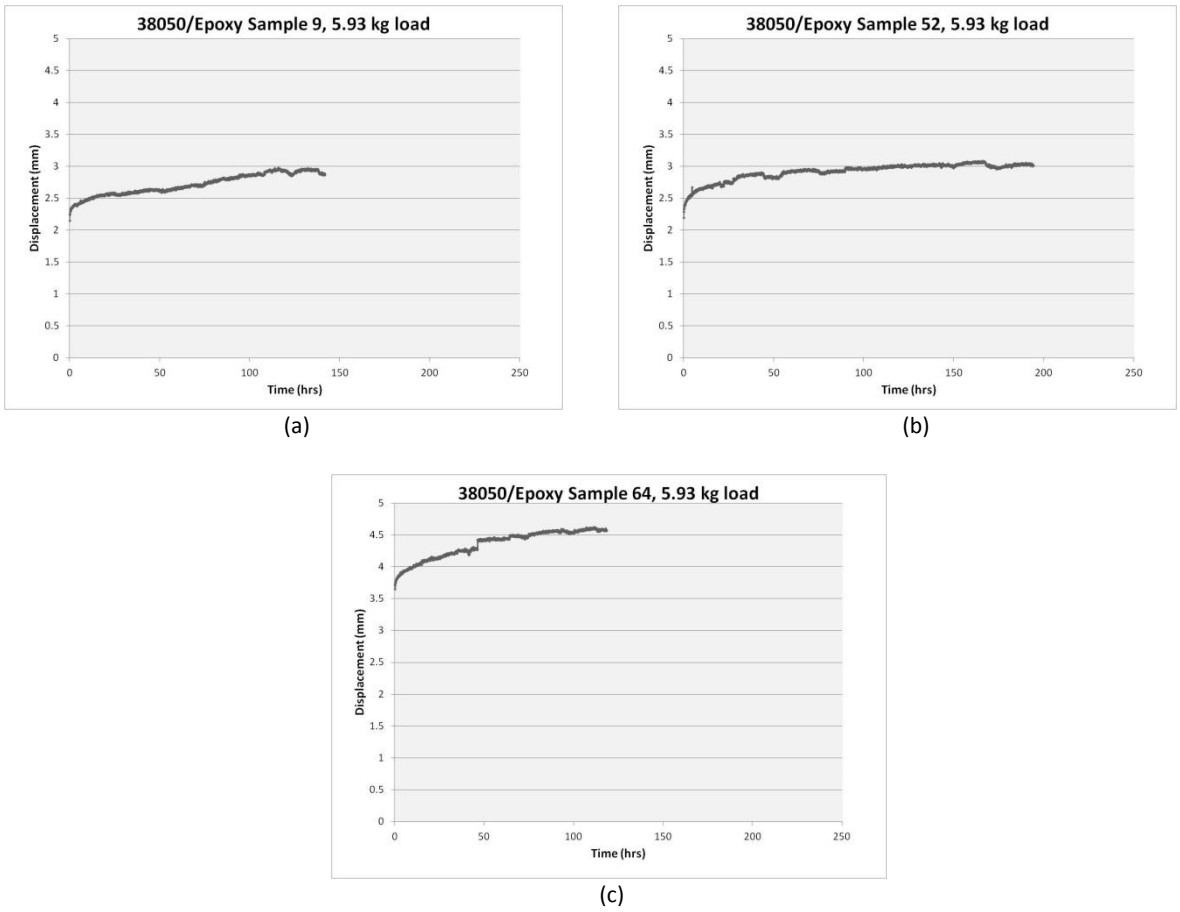

Figure AII. 3. Individual constant load creep results at room temperature for 38050/Epoxy samples.

APPENDIX II: CREEP DATA

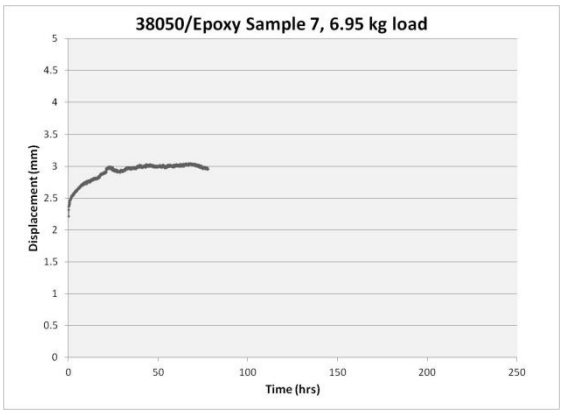

(d)

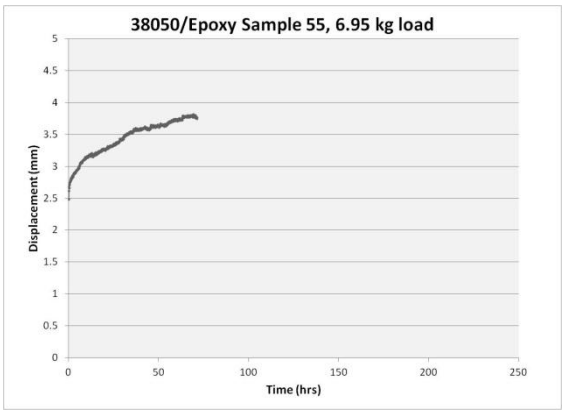

(e)

Figure AII. 3 cont. Individual constant load creep results at room temperature for 38050/Epoxy samples.

APPENDIX II: CREEP DATA

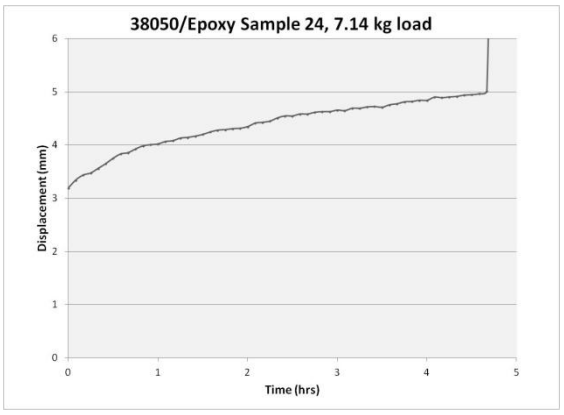

(f)

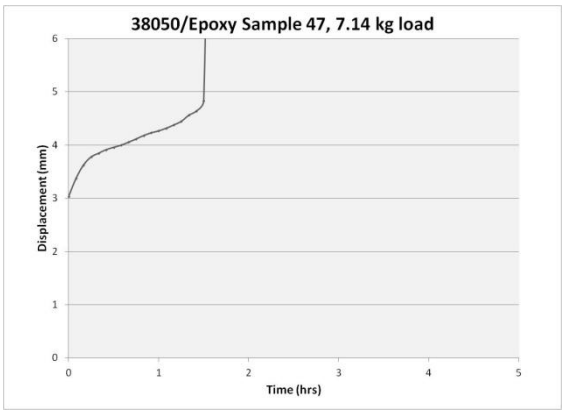

(g)

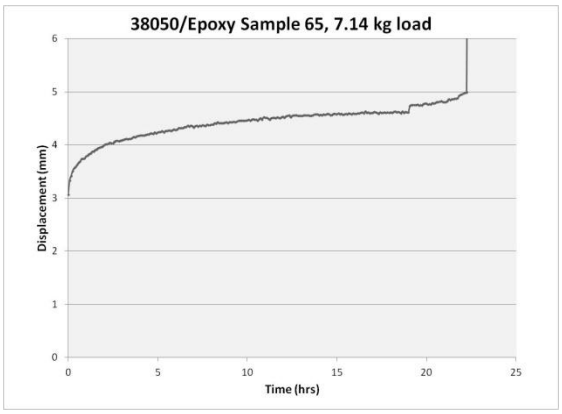

(h)

Figure AII. 3 cont. Individual constant load creep results at room temperature for 38050/Epoxy samples.

APPENDIX II: CREEP DATA

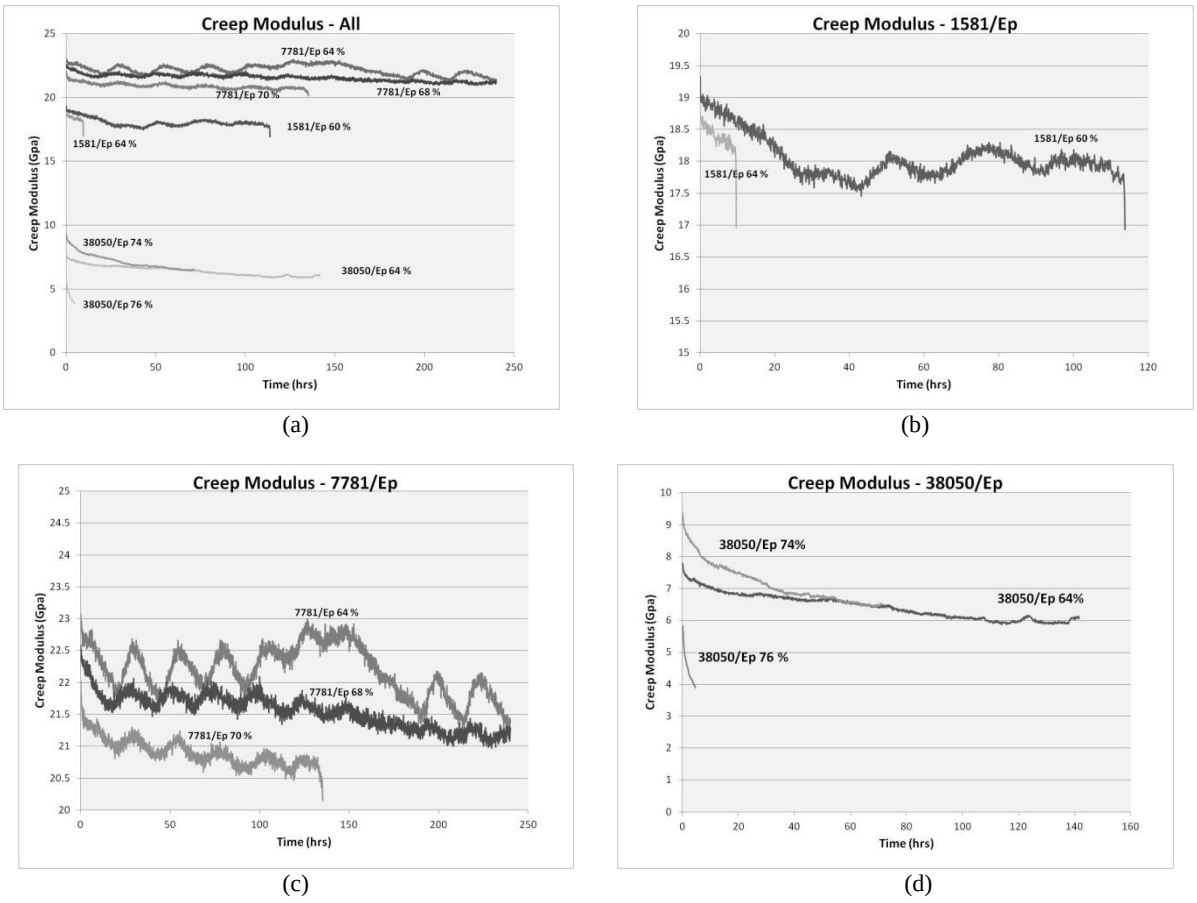

Figure AII. 4. Uncorrected creep modulus curves with data recorded every five minutes.

Vita

Carolyn Kidwell was born in Terre Haute, Indiana on August 5, 1987, daughter of James and Barbara Kidwell. She has lived in many places throughout the United States due to her mother's career at Alcoa, Inc. Currently she resides in Knoxville, Tennessee. At the University of Tennessee, she earned her Bachelors of Science (2009) and Masters of Science (2012) in Materials Science in Engineering. A portion of this thesis was published in the Journal of Composite Materials during her time in the master's program at UTK.